國立交通大學

應用化學系碩士班

碩士論文

雷射捕捉誘發水中 PNIPAM 分子相轉變動態之研究藉由光學顯微技術及時間分析螢光顯微光譜技術

Laser-induced phase transition dynamics of poly(N-isopropylacrylamide) in water studied by optical microscopy and time-resolved fluorescence microspectroscopy.

研究生：曾祭績　(Tseng Chin-Hsu)

指導教授：三浦篤志 博士 (Atsushi Miura)

中華明國 一百零一年 七 月

Abstract

Student：Tseng Chin-Hsu Advisor：Dr. Atsushi Miura

M. S. Program, Department of Applied Chemistry
National Chiao Tung University

A poly(N-isopropylacrylamide) (PNIPAM) is famous thermo-responsible polymer which shows phase transition above lower critical solution temperature (LCST). PNIPAM collapses into globule from coli state where hydrated water molecules are excluded from the polymer matrix. It is considered that the phase transition behavior including dehydration process and folding change is a good example of biological polymers such as protein, therefore many studies of phase transition behavior of PNIPAM have been examined for more than couple of decades. However direct molecular dynamics of phase transition of PNIPAM is few. In this study, we studied molecular spectroscopic phase transition dynamics of PNIPAM by introducing laser trapping, optical microscopy and time-resolved fluorescence microspectroscopy with fluorescently labeled PNIPAM. We induce local phase transition around the focal spot of trapping laser by tight focusing of trapping light source under microscope. Laser-induced phase transitin behavior and its dynamics was visualized by combining with steady state and time-resolved spectroscopy.

Studies on a trapping-induced phase transition behavior of PNIPAM in different

aqueous solvents, H_2O and D_2O, revealed that clearly different phase transition behavior. Trapping laser irradiation induced spherical particle formation at the focal spot. The size and formation time strongly depends and changes upon solvent and laser power. It is interpreted due to a thermal effect caused by an absorption of irradiated trapping laser light by the solvents. Larger absorption coefficient of H_2O than D_2O enables the phase transition at lower laser power in former solution.

Based on the information of phase transition dynamics obtained by non-labeled PNIPAM, we examined phase transition dynamics of fluorescently labeled VDP-PNIPAM. Fluorescence microscopy and microspectroscopy results of phase transition dynamics of VDP-PNIPAM clearly indicate the molecular environmental change from coli to globule during phase transition with showing the peak wavelength shift of fluorescence spectra. In addition to the fluorescence spectrum under laser trapping-induced phase transition, we measured fluorescence decay during and after phase transition. Analysis of fluorescence decay curves showed the change of decay component during phase transition which also reveal dynamic change of molecular environment during phase transition.

Additionally we found an unusual two color lasers induced phase transition behavior when we introduce weak ultraviolet (UV) laser simultaneously with near infrared (NIR) trapping laser. A spherical particle formed by trapping laser irradiation

showed an expansion of its size when an additional weak UV light was introduced. Observed two-color laser irradiation-induced particle size expansion will be interpreted by two reasons at the moment; resonance effect and photothermal effect.

雷射捕捉誘發水中 PNIPAM 分子相轉變動態之研究藉由光學顯微技術及時間分析螢光顯微光譜技術

研 究 生：曾綮續　　指導教授：三浦篤志博士

國立交通大學 應用化學系碩士班

中文摘要

聚(N-異丙基丙烯醯胺)(PNIPAM) 是有名的熱反應性聚合物, 當溫度高於臨界溶液溫度(LCST)時會發生相轉變.PNIPAM 的分子結構會因水分子被排除掉而從直鏈狀聚成球狀. 我們認為這個相轉變的過程是一個相當好的生物聚合物,例如:蛋白質的研究範例因其中包含了去除水分子及分子鏈摺疊改變, 因此在過去的幾十年中已經有許多相轉變現象的研究. 然而,直接的相轉變動態的研究仍是相當稀少. 在這項研究中,我們利用雷射捕捉誘發相轉變結合分子光學來研究相轉變動態及時間解析顯微螢光光譜來研究螢光標定的PNIPAM 分子. 藉由結合靜態及時間解析光譜, 我們可以觀測雷射捕捉誘發相轉變及其動態變化.

研究雷射捕捉誘發 PNIPAM 相轉變於不同溶液中, H2O 及 D2O, 確實透露出不同的相轉變過程. 雷射捕捉會誘發球形粒子於雷射聚焦點. 大小及形成時間與溶劑及雷射強度相當有關以及會隨之改變. 這個結果說明了因溶劑吸收雷射而產生的熱效應. H2O 的吸收係數比 D2O 大以致於相轉變可以藉由較小強

度的捕捉雷射來成形.

以未標定的PNIPAM 相轉變動態過程為基準,我們觀測了被標定的PNIPAM 分子,VDP-PNIPAM, 的相轉變動態過程. 藉由觀測光譜波長峰值的位移,螢光顯微及顯微光譜上的結果清楚指出了 VDP-PNIPAM 相轉變動態過程中,分子環境從直鏈狀變為球狀的改變. 除了測量在雷射捕捉誘發相轉變條件下的螢光光譜,我們也在過程中及結束後測量螢光強度衰退. 分析相轉變過程的螢光強度衰退也透露出了分子環境在向轉變過程中的動態改變.

除此之外,我們發現了一個不同於以往的雙色雷射誘發相轉變現象,當我們同時引入紅外光捕捉雷射與一道較弱的紫外光雷射. 當額外的弱紫外光雷射引入時,藉由雷射捕捉所形成的球形粒子會大小上會發生擴張的現象. 在現階段,這項雙色雷射誘發相轉變大小擴張的現象會以兩個說法來解釋, 共振效應及光轉熱效應.

List

List of Figure

List of Table

1. Introduction

To study dynamic structural change or phase transition of biological molecules, it is indispensable to understand conformational and hierarchic structure change at molecular level during its function emerging process with high space- and time-resolution. For instance, protein structure can be represented by α-helix, β-sheet, and so on by changing surrounding condition such as temperature, pressure, salt and enzyme concentration, and electric potential of membrane etc. However direct investigation of structural transition dynamics is experimentally hard, thus varieties of stimuli-responsive polymers have been used for such kind of studies. A poly(N-isopropylacrylamide) (PNIPAM) is one of such stimuli-responsive polymer.

As is well established, PNIPAM in aqueoussolution exhibits a structural change upon increasing the temperature beyond a lower critical solution temperature (LCST) at 32˚C. [1] As a consequence, NIPAM solutions show phase transition above the LCST. This fascinating thermo-responsive behavior stimulated extensive studies of PNIPAM solutions and gels for the preparation of stimuli-responsive devices and formulations with potential biomedical applications.[2, 3]

A molecular mechanism behind the phase transition of PNIPAM is considered due to the dehydration in the polymer matrix and, therefore, less hydrogen bonding

between amide moiety and water molecule which renders water a poor solvent for the chain. Hence, the polymer chain existing as an extended coil collapses into a globular form above the LCST with a high degree of tight contact among the hydrophobic side chains. As established primarily by calorimetric studies, [4, 5] the PNIPAM chain in the collapsed state is composed of globular domains of a size in the order of molecular weight (MW ~10^4) with small extended portions of the chain in between them. This scenario is well supported by a wealth of experimental results by light scattering [6, 7], NMR [8-10] and fluorescence spectroscopies [11, 12]. Macroscopically, the solution turns turbid above the LCST, even for short (MW ~10^4) chains of PNIPAM.[13, 14] This latter observation indicates that intermolecular aggregation also occurs, a scenario that is further corroborated by elegant fluorescence experiments [15] with doubly labeled polymer chains and by detailed light-scattering studies.[16, 17] There are also indications that at finite concentrations of PNIPAM can form stable multi-chain aggregates which are reported to as ‘‘mesoglobules’’.[18, 19]

In contrast to the wealth of observations underlying the broad structural consensus, there is a remarkable lack of understanding of PNIPAM phase transition on the time course of molecular events in the bulk solutions. Quite little is known about the dynamic behavior of phase transition and separation of PNIPAM. Kinetic studies were performed in the dense (5–90 wt.%) regime by calorimetry investigations

indicated a demixing/remixing process that may proceed on the <100 s time scale with the remixing being slower than the demixing [20] and ultrasonic attenuation studies revealed dynamics of ambiguous origin on the minutes-to-hours time scale.[21]

In 2006, Yushmanov et al. performed a temperature-jump 1H NMR study on PNIPAM to access the dynamic behavior of the phase transition/separation in an aqueous polymer solution (1wt.%).[22] Their results revealed that phase mixing/demixing, i.e. phase separation, was completed within a few seconds. In order to elucidate a dynamic behavior of the phenomena, however, further detailed investigation with better time resolution is necessary. Tsuboi et al. reported that the phase separation dynamics of PNIPAM in aqueous solutions by means of a laser temperature-jump (T-jump) technique.[23] They revealed that the time constant of the phase separation of the polymer solution was proportional to the square of the hydrodynamic radius of the polymer.

However direct spectroscopic approach to study the phase transition dynamics of polymer solutions is usually difficult, since coiled and globular states are hardly distinguished spectroscopically. To overcome this experimental difficulty, we employ a PNIPAM co-polymerized with fluorescent probe in this study [24-26]. A use of a fluorescent probe molecule is effective for studying the molecular motion of PNIPAM

systems, as Winnik et al. have demonstrated previously.

1.1 Poly(N-isopropylacrylamide) (PNIPAM) and its phase transition behavior

PNIPAM is one of the most widely studied thermoresponsive polymer. PNIPAM is a chemical isomer of poly-leucine, in that it has the polar peptide group in its side chain rather than in the backbone.[27] PNIPAM consists of a hydrocarbon backbone with hydrophilic and hydrophobic moieties in the form of carboxyl, amide and isopropyl groups as shown in Figure 0.1 Chemical structure of PNIPAM.. In aqueous solution, PNIPAM displays a LCST at 32˚C; at this temperature it undergoes a sharp and reversible coil-to-globule phase transition from a hydrophilic to a more hydrophobic state, forcing water out from the matrix. This phenomenon occurs due to the domination of entropic effects (displacement of water from the polymer matrix) over enthalpic effects (formation of hydrogen bonds between polymer and water molecules) as the temperature increaes above the LCST.[28, 29]

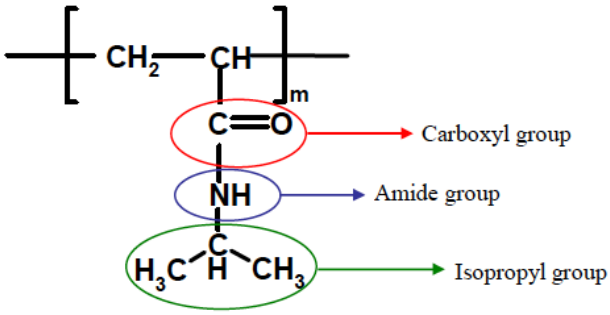

Figure 0.1 Chemical structure of PNIPAM.

Below LCST, PNIPAM chains exist in an extended coil conformation, and solvation is driven by the enthalpic gain from intermolecular hydrogen bonding between the PNIPAM chains and water molecules as shown in left side in Figure 0.2.[2] As the temperature is increased towards the LCST, intramolecular hydrogen bonding between carboxyl and amide groups on the PNIPAM chains result in the interruption of hydrogen bonding of these groups with water molecules, ultimately resulting in the chain adopting a collapsed conformation, driving out the water, and causing the polymer to precipitate in the solution as shown in right side in Figure 0.2. These interesting properties of PNIPAM and its copolymers make them applicable to a diverse range of pharmaceutical and biomedical applications [30, 31].

Coil state:
Before phase transition

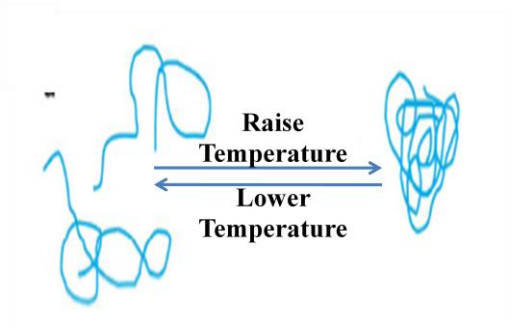

Globule state:
After phase transition

Figure 0.2 Schematic drawing of PNIPAM phase transition.

Recent works by Masuhara and his colleagues demonstrated that phase transition of PNIPAM can be induced not only thermally but also optically. In their photo-induced phase transition studies, they applied laser trapping in which a photon pressure induced by tight focusing of intense laser beam. Laser trapping induced phase transition was first demonstrated by Ishikawa et al. where a single PNIPAM microparticle formation/disappearance by turning on/off of a focused near infrared (NIR) laser beam under an optical microscope [32]. Induced phase transition is explained by local heating around the laser spot since H_2O has an overtone absorption band at NIR region. When the trapping laser was introduced into solution, the hydrogen bond between solvent and polymer will be corrupted by heating and then the polymer will become like a small single particle. Radiation force caused by focused laser beam will collect these particles and trapped particles are assembled and forming spherically-shaped microparticle at the focal spot as schematically depicted

in Figure 0.3.

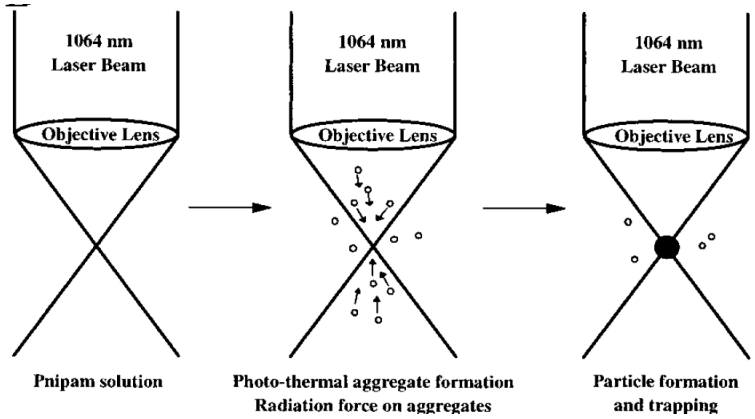

Figure 0.3 Focus laser beam induced molecular assembly formation of PNIPAM in aqueous solution. Figure from reference [33]

The following work was done by Hofkens et al. [34] who used D_2O as solvent to suppress the absorption of the overtone of O-H stretching band. D_2O has less absorption at 1064 nm and temperature elevation can be drastically suppressed; thus thermal phase transition is prevented under examined condition. Even using D_2O as solvent, they succeeded to induce microparticle formation due to the phase transition. It means that photon pressure induced by tight focusing of trapping laser light can collect molecule around the focal spot and form molecular assembly with non-contact, non-invasive and non-destructive manner with trapping and manipulation of molecules and molecular clusters. Thus, laser trapping technique is very good method for studying phase transition dynamics under photon pressure by combining

conventional optical microscopy such as bright field imaging, fluorescence imaging, fluorescence spectroscopy and lifetime imaging microscopy.

1.2 Laser trapping

Laser trapping is a very powerful technique which is widely applied in many research field, such physics, chemistry, biochemistry and biology. This tool is advantageous to manipulate micrometer particle freely without contact directly by focused intense laser light.

1.2.1 History of laser trapping

In early 1970s, Ashkin et al. demonstrated that optical forces could manipulate micron-sized dielectric particles in gas phase and liquid.[35] They identified two forces exerted to the object under photon pressure: a scattering force which work in the direction of the incident light beam and gradient force which pointing in the direction of the intensity gradient of laser beam.[36] This investigation led to the development of the single-beam gradient force optical trapping and was applied to wide range of objects from neutral atom to biological molecules. This unique technique has a revolutionary impact in broad area of science which mainly

discussing about single particle. In biology, it was used to study folding and unfolding of DNA, bacterial motion, and an activity of molecular motors.[37] Also in other area, an optical tweezers is a powerful tool especially for three dimensional manipulation of micrometer-particle. Masuhara *et al*. performed the experiments combining optical trapping with several microscopic techniques as fluorescence, absorption spectroscopy, photochemistry and electrochemistry.[38] Recently they have been applying this technique to induce a crystallization of biological molecules.[39]

By focusing a laser beam tightly with high numerical aperture (NA) objective lens, the dielectric particle will experience a force due to the momentum transfer from scattered photons as shown in Figure 0.4.[40-42] This trapping force can be decomposed in two components; (1) scattering force and (2) gradient force. The scattering force is in the direction same as light propagation, meanwhile the direction of gradient force is same as the direction of spatial light gradient. For the stable trapping, the axial gradient force should be larger than scattering force, then light can collect particles to the focal spot. This condition can be satisfied by using high NA objective lens which enables to make a diffraction limited spot size by sharp focusing of laser beam.

For theoretical treatment, there are two limiting cases needed to be considered.

First, the particle radius (r) is larger than the trapping laser wavelength (λ), ($r >> \lambda$). In this condition, it will be considered as Mie scattering regime and the optical forces exerted to the particle can be handled with ray optics (Figure 0.4). By Newton's third law, the momentum change of incident photon is equal to the momentum change of particle and the direction is opposite. The force induced by momentum change is proportional to the light intensity. If the refractive index of spherical particle is larger than that of surrounding medium, the direction of the force matches to the direction of intensity gradient. Vise versa, if the refraction index of particle is smaller than that of medium, then the direction will be opposite. Thereofore, the first condition can trap the particle at the focal spot of the trapping laser and the second cannot.

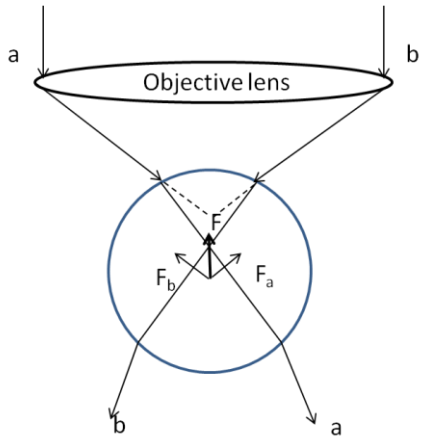

Figure 0.4 Schematic diagram of ray optics for typical trapping which the refraction index of particle is larger than that of the medium. Redraw from [42].

Second, the particle is far smaller than the trapping laser wavelength ($r << \lambda$) [40]. In this case particle can be treated as Rayleigh particle. We can treat the particle as point dipole for the calculation of working force to the particle. The force can be written as below;

$$F = \frac{1}{2}a\nabla E^2 + a\frac{\partial}{\partial t}(E \times B) \text{.....1.1,}$$

$$a = 4pe_b g^3 \frac{(n_a / n_b)^2 - 1}{(n_a / n_b)^2 + 2} \text{.....1.2.}$$

Here, the E and B in equation 1.1 mean electric field and magnetic flux density, r means the radius of spherical particle which. α is polarizability. n_a and n_b mean the refraction index of particle and medium. The first and second terms of eq. 1.1 mean gradient and scattering force, respectively. When $n_a > n_b$, the direction of gradient force is in direction of light intensity. For a focused NIR laser beam, the gradient force is usually larger than the scattering force which leads a stable trapping of the particle at the focal spot.

1.3 Fluorescence microscopy/spectroscopy for phase transition dynamics study

Steady-state and time-resolved fluorescence spectroscopy have been very powerful tool for molecular spectroscopic investigation of fluorescent molecules in

condensed phase. During a couple of decades it has grown dramatically due to the development of new optics, detectors, methods, and combing with different measurement systems such as microscopy, and we can detect very tiny signal from a single molecule. Fluorescence spectroscopy and time-resolve fluorescence measurement have already been very useful tool for the imaging of molecular dynamics in chemical, physical, and biological systems with single-molecule level. Fluorescence technique is used in so many applications, two-photon excited fluorescence (TPEF), fluorescence correlation spectroscopy (FCS) and so on. By introducing and combining with these techniques, fluorescence measurements can provide further information on a wide range of molecular process, such as intramolecular interaction, rotational diffusion, conformation changes, and binding interaction in biological systems, and also light induced phase transition dynamics.

We will construct fluorescence lifetime imaging microscopy system to investigate dynamics of phase transition of PNIPAM under laser trapping condition. More details will be discussed in latter section.

1.4 Aim of this study

As we mentioned before, phase transition of PNIPAM can be induced by trapping laser focusing in solution. In this study, we aim to clarify laser trapping induced phase

transition dynamics by using fluorescently labeled PNIPAM molecule, 3-(2-propenyl)-9-(4-N,N-dimethyl-aminophenyl-phenanthrene)-co-poly(N-isoproylacrylamide) (VDP-PNIPAM). As we mentioned above, the use of a fluorescent probe molecule is effective for studying the molecular motion of PNIPAM systems, as Winnik et al. have demonstrated in previous. We constructed fluorescence microscopy/spectroscopy system which is based on wide-field fluorescence and bright field microscope for the visualization of phase transition dynamics. We also constructed stage-scanning fluorescence lifetime imaging microscopy system to investigate photon pressure induced phase transition dynamics with more quantitative approach.

In addition to these phase transition dynamics study, we have found interesting novel phase transition behavior of PNIPAM derivatives. We found unusual two color laser induced phase transition under laser trapping; an introduction of weak UV light induces further phase transition. Although photon density of second UV laser is much weaker than that of trapping laser by 8 to 10 orders of magnitude, phase transition expansion when trapping laser power is higher than the threshold occurred very efficiently. We will also study phase transition dynamics of this unusual behavior and discuss from molecular spectroscopic view points.

2. Experiment

2.1 Materials

Deionized water prepared with water purifier system (Sartorius, sarui611DI) and deutarated water (D_2O, >99%) purchased from Sigma-Aldrich was filtrated with a syringe filter (pore size; 0.22 mm, SLGV 013 SL, Millipore) before usage. Poly-(N-isopropylacrylamide) (PNIPAM, >99%, average molecular weight: 1.9 ~2.2 $x10^4$) was purchased from Sigma-Aldrich and used without further purification. Its structure is shown in Figure 2.1a.

For fluorescence microscopy and spectroscopy of one and two color laser induced phase transition, an intramolecular fluorescent probe, which is 3-(2-propenyl)-9-(4-N,N-dimethyl-aminophenyl-phenanthrene) (VDP), was used. Structure of VDP-PNIPAM is shown in Figure 2.1b. VDP-PNIPAM was prepared by radical polymerization as reported elsewhere.[43, 24, 26] Its molecular weight is about $3.0x10^4$ which was determined by size exclusion chromatography. It contains 0.1 mol% of VDP unit: namely only one VDP unit is included in a single PNIPAM chain.

Sample solution was prepared by adding a solvent to powder polymer sample (PNIPAM and VDP-PNIPAM) and left for over night at room temperature to ensure that polymer was totally dissolved solution. A concentration of PNIPAM and

VDP-PNIPAM solution for trapping experiment was adjusted to 3.5 wt% both for H_2O and D_2O cases.

Steady state absorption and fluorescence spectra of the sample were measured by absorption spectrophotometer (V-670, Jasco) and fluorescence spectrophotometer (F-4500, HITACHI)

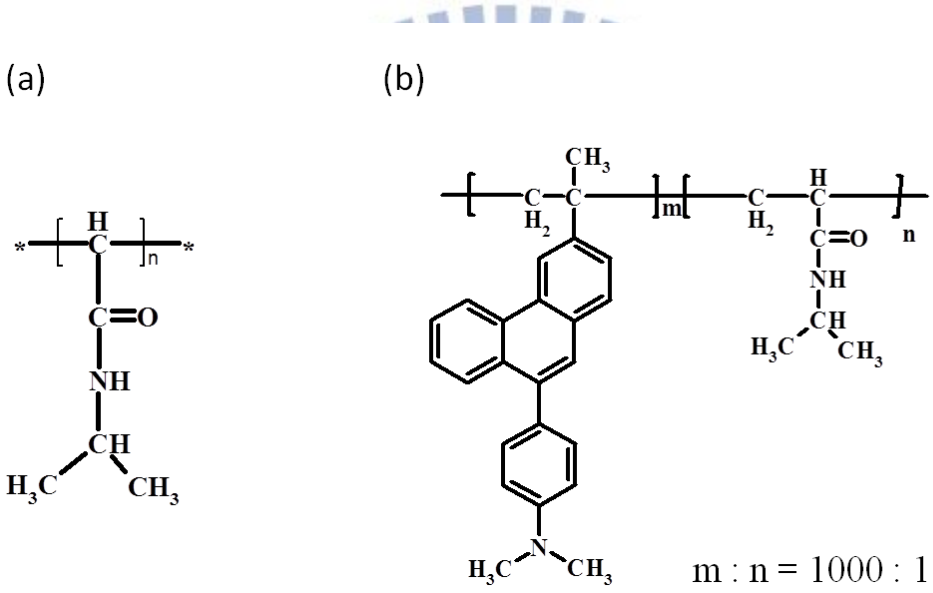

Figure 2.1 Chemical structure of (a) PNIPAM and (b) VDP-PNIPAM)

2.2 Bright field transmission imaging and fluorescence imaging/spectroscopy system:

Laser trapping-induced phase transition behavior of PNIPAM and VDP-PNIPAM was observed by microscopy system which depicted in Figure 2.2a. The laser trapping

microscopy system used in this study is based on an inverted microscope (IX71, Olympus) equipped with double backport. We can introduce two different light sources easily to the microscope objective lens with this configuration. A near-infrared NIR laser beam of continuous wave (CW) Nd:YVO_4 laser (Matrix 1064-10-CW, Coherent) at the wavelength of 1064 nm was used as a trapping light source. Trapping laser was focused into the sample solution in sealed glass chamber through an objective lens (40X, N.A.: 0.95). Trapping laser power was adjusted to 100 mW ~ 1.2 W at sample position by using variable neutral density filters. It should be noted that all the laser power mentioned in this study was measured value through objective lens.

Prepared PNIPAM and VDP-PNIPAM sample solutions were placed in a homemade sealed glass chamber which was made by sandwiching piled parafilm with two cover glasses (24 mm x 30 mm, 100 μm thickness, Gold Seal) as shown in Figure 2.2b. The cover glass was cleaned by detergent and potassium hydroxide solution for several times prior to use for chamber fabrication. The thickness of the sample chamber was adjusted by piling parafilm where the average distance between two cover glasses is ~90 μm. Focusing position of the trapping laser was set to 10 μm lower than the bottom surface of upper cover slip; i.e. 80 μm from the bottom glass substrate surface.

Laser trapping-induced phase transition was recorded by bright field transmission imaging with using a halogen lamp as light source and CCD and EMCCD camera as for the detector.

We also performed wide-field fluorescence imaging of phase transition behavior. We used 325 nm line of CW He-Cd laser (IK-3401R-F, Kimmon) and, 405 nm CW diode laser (Cube 405-100C, Coherent) as for fluorescence excitation light source. In addition to these CW lasers, we also used second harmonic (SH) of femtosecond Ti:Sapphire laser (Tsunami, Spectra Physics) operated at 750 nm where we can obtain 375 nm second harmonic generation (SHG) output as for excitation light. This pulsed laser was also used in fluorescence lifetime experiments and more details are mentioned later. Excitation laser beams at 375 and 405 nm were introduced coaxially from the bottom of the sample thorough the same objective lens as well as trapping laser as depicted in Figure 2.2a. Fluorescence excitation laser beams were focused to the back imaging plane of objective lens to achieve collimated light after objective lens. Collimated light can irradiate more than ~150 μm observation field under microscope and it is sufficiently wide for our observation. In contrast, a 325 nm excitation light was introduced to the sample from the above without using objective lens since transmission efficiency of microscope objective at this wavelength is too low to obtain sufficient power density for wide-field fluorescence imaging. Beam spot

size of 325 nm is ~ 3 mm at the sample position. luorescence signal was detected by EMCCD camera (PhotonMAX, Princeton instruments).

Fluorescence signal was divided into two path by introducing beam splitter in the detection optical path as shown in Figure 2.2a. One of the light path was used for the spectrum measurement which passed through confocal pinhole placed in an optically conjugated plane of a focal plane of objective lens. Therefore we can detect the fluorescence signal merely from a focal spot. The light passed through the confocal pinhole was focused to the entrance slit of spectrograph (MS125, Oriel) equipped with cooled CCD (i-Dus DU401A-BR-DD, Andor) to obtain fluorescence spectra. By using this fluorescence microscopy/spectroscopy setup, we can examine simultaneous wide-field fluorescence imaging and confocal fluorescence spectroscopy of the molecules trapped under exerted photon pressure.

All the trapping experiments were carried out at room temperature (25°C) and 50~60% of humidity condition.

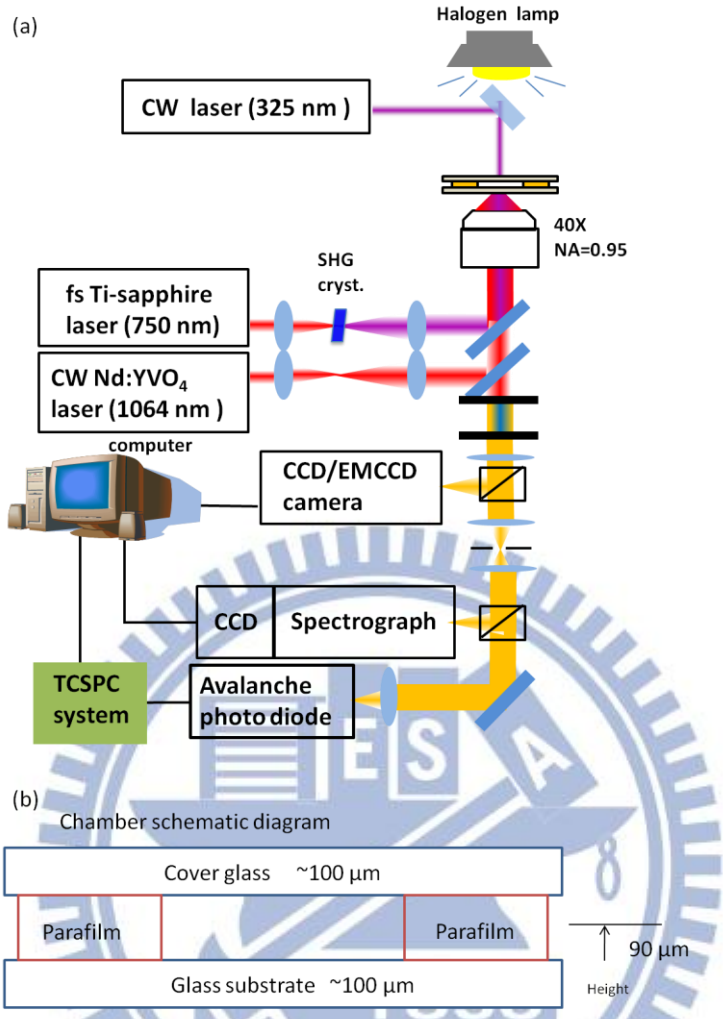

Figure 2.2 (a) Schematic diagram of microscope setup for bright field transmission imaging and wide-field fluorescence imaging/spectroscopy. (b) A drawing of sealed glass chamber.

2.3 Microscopy setup: Fluorescence lifetime imaging microscopy system

Fluorescence lifetime of the molecules will give more useful information about molecular dynamics of laser trapping-induced phase transition. We have carried out

fluorescence lifetime observation of fluorescently labeled VDP-PNIPAM in addition to fluorescence imaging and spectroscopy. We used CW Nd:YVO_4 laser (Millenia X, Spectra Physics) pumper mode-locked femtosecond Ti:Sapphire laser (Tsunami, Spectra Physics) as excitation light source of fluorescence lifetime measurements. The output wavelength of this laser can be adjusted from 700 to 980 nm. To excite VDP moiety with SHG, operation wavelength was adjusted to 750 nm. Repetition rate, maximum output power and pulse width at 750 nm are 80MHz, 800 mW and ~150 fs. Fundamental output from Ti:S oscillator was introduced to a pulse selector (Model 3980, Spectra Physics) in which an acousto-opitc modulator (AOM) thinned out pulses from the pulse train to change the repetition rate.

We took a SHG by focusing fundamental after passing pulse picker and obtained 375 nm excitation light. A SHG of Ti:S laser was introduced into the objective lens coaxially with NIR trapping laser to excite the molecules from the different back port of the microscope as depicted in Figure 2.3. Emission from the sample was corrected by the same objective lens and brought to an optical fiber which is connected to a single photon counting avalanche photo diode (APD) (SPAD, Micro Photon Device) after passing the confocal pinhole. Thus, obtained fluorescence lifetime is basically from the confocal volume and can obtain with high spatial resolution. Fluorescence signal passed a set of filters to eliminate unwanted scattering light from excitation

laser light, environment and sample prior to introduce to the APD. The fluorescence emission collected by the APD was coupled into an in-house assembled time-correlated single photon counting system to construct the lifetime decay histogram. Data collection was controlled by PicoHarp 300 TCSPC system (PicoQuant). Detailed diagram of TCSPC system is shown in Figure 2.4. In short, converted signal of emission was sent from APD to signal router (PHR 800, PicoQuant). Signal router transfers the APD signal as decay signal to photon counting module. A reference signal to construct fluorescence decay histogram, an oscillating laser signal detected by fast photodiode (818-bb-21, Newport) was brought to the photon counting module, and used to construct by calculating the difference of arrival timing as we explained about a principles of TCSPC in a previous section. Instrument response function (IRF) was generated by collecting scattered laser light from a colloidal scattering solution (Ludox CL-X colloidal silica 45 wt% suspension in water, Sigma-Aldrich). Lifetimes were measured at the emission wavelength of VDP and in each case data were collected until 10,000 counts in the channel of maximum intensity. Then, fluorescence lifetimes were extracted from the measured decay curves using FluoFit (PicoQuant) which implements nonlinear least-squares error minimization analysis, based on the Simplex and Lavenberg-Marquardt algorithms. The final quoted result was determined by the fit, which had a χ^2 value of less than 2.0 and

residual trace that was symmetric about zero.

As shown in Figure 2.3 constructed fluorescence lifetime measurement system is integrated with fluorescence imaging/spectroscopy system. Therefore we can perform simultaneous fluorescence lifetime measurement, fluorescence imaging and spectroscopy. It is quite advantageous to study the phenomena that occur with hierarchic dimension such as phase transition.

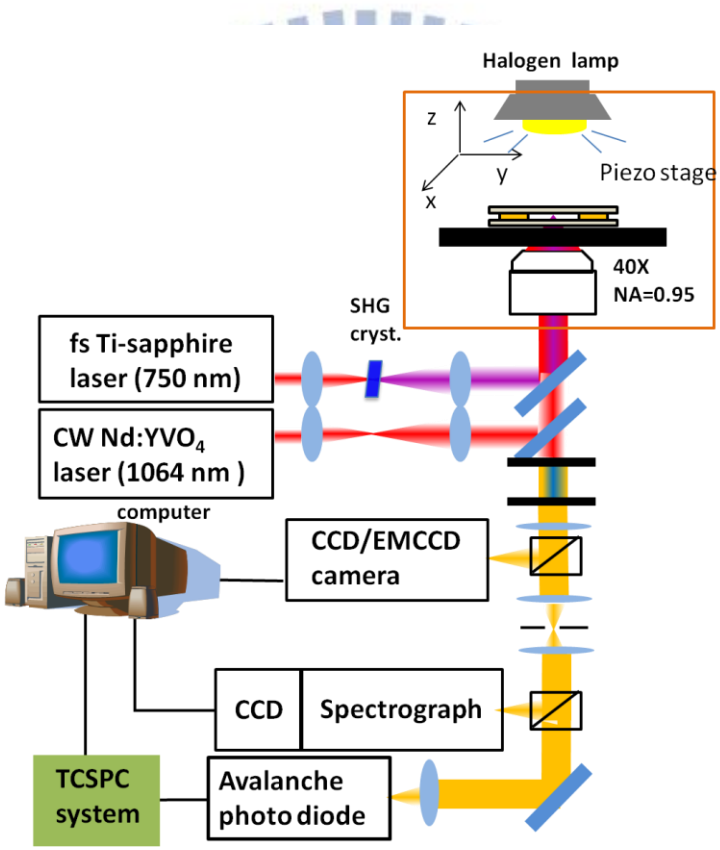

Figure 2.3 Schematic diagram of fluorescence lifetime imaging microscopy

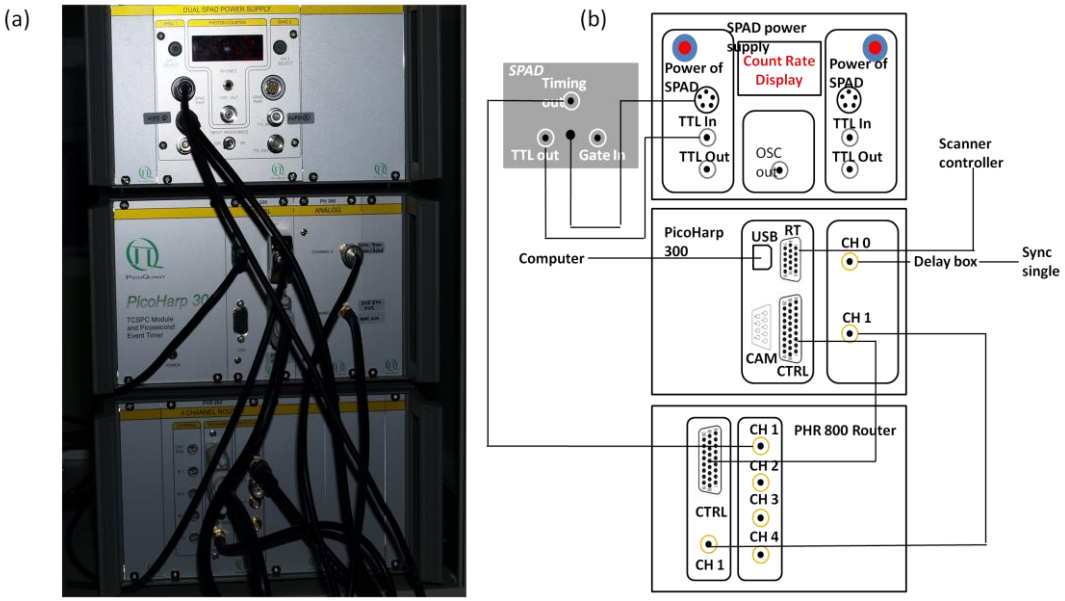

Figure 2.4 System of fluorescence measurement: (a) A picture of TCSPC system and (b) cabling diagram.

3. Phase transition of PNIPAM induced by trapping laser

As we described in a previous section, we can induced phase transition of PNIPAM by focusing trapping laser. Temperature elevation will cause macroscopic phase transition of PNIPAM solution, meanwhile focused trapping laser beam induces microparticle formation at the focal spot due to the phase transitions. We will use non-labeled PNIPAM to find suitable experimental conditions for phase transition dynamics study of fluorescently labeled PNIPAM.

3.1 Laser trapping-induce phase transition of PNIPAM

Local phase transition induced by focused NIR laser beam can be considered in two reasons, thermal effect of NIR laser by the vibronic absorption of solvent and photon pressure. To clarify these two effects, we prepare the sample with D_2O solution to suppress the absorption of NIR laser.

The results of laser induced phase transition in H_2O and D_2O at the same trapping laser power (725 mW) were shown in Fig. 3.1. In both solution conditions, we could observe particle formation depend on applied laser power and it disappeared by terminating trapping laser irradiation as well as previous report.[33] However, obtained results showed drastic different in both phase transition particle size and particle formation time depending upon the solvent even though trapping laser power

was the same.

The particle formed in H_2O solution was larger than that formed in D_2O under same laser power as shown in Figure 3.1. Average diameter of the particle formed in H_2O (~14 μm) at 725 mW of trapping laser power was almost twice of that formed in D_2O as mentioned in Table 3.1. Particle size became larger with increasing the laser power more than the size of view field size of EMCCD under microscope (more than 60 μm) in H_2O. In contrast, maximum size saturated around 10 μm in D_2O. Formed particle size became obviously lager in H_2O when the laser power was higher than 600 mW as shown in Figure 3.2.

Particle formation time, which is defined as a necessary time to generate a microparticle due to phase transition, was also clearly different between H_2O and D_2O. Particle formation time became shorter with increasing the laser power as shown in **錯誤! 找不到參照來源。**. Particle was formed almost immediately after starting irradiation more than 600 mW laser power in H_2O, meanwhile it needed about 10 min at the same laser power in D_2O (Table 3.1).

We restricted the observation time for 30 min to determine power threshold of phase transition. We observe quite rapid phase transition even at 200 mW in H_2O, but PNIPAM in D_2O could not show phase transition less than 425 mW within 30 min. Power density at 425 mW is caluculated from theoretical diffraction limited beam spot

size and NA of used objective lens (NA=0.9) to be ~50 MW/cm^{-2}. Therefore we can define phase transition threshold power density in D_2O is ~50 MW/cm^{-2}. On the other hand, threshold power density in H_2O can be said less than 25 MW/cm^{-2} under examined condition.

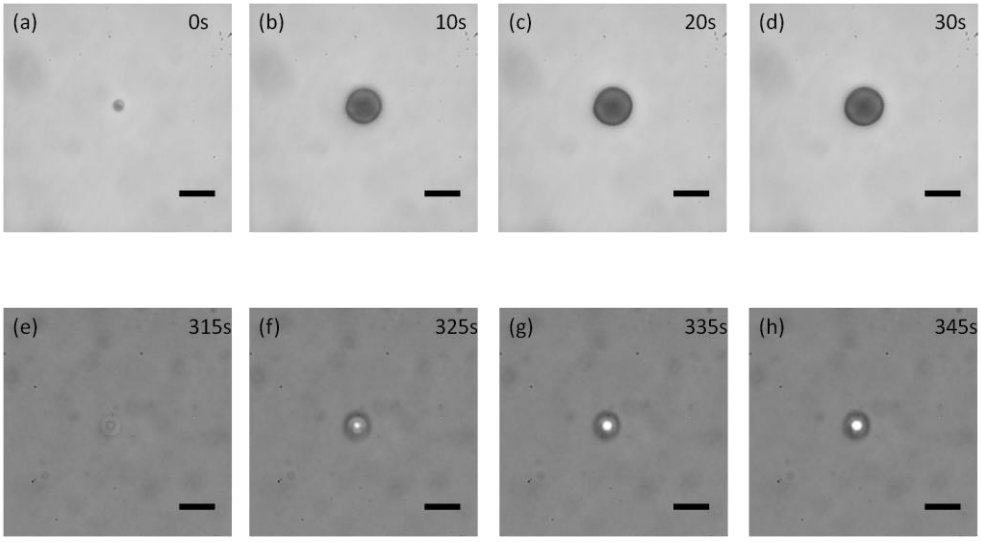

Figure 3.1 Local phase transition induced by laser trapping in (a) ~ (d) H_2O and (e) ~ (f) D_2O. Laser power was 725 mW. Scale bar = 10 μm. Time indicated in the images corresponds the irradiation time of trapping laser.

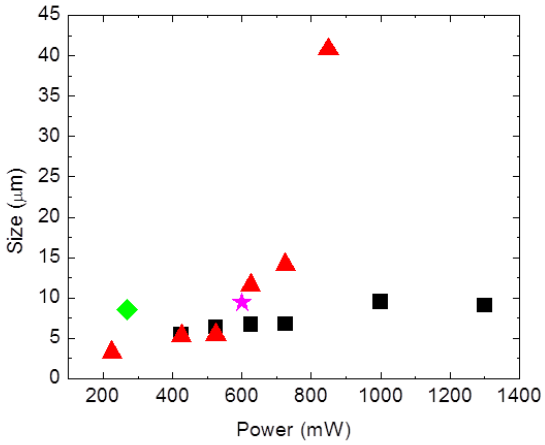

Figure 3.2 Trapping laser power dependent formed particle size difference. The symbols show PNIPAM in H_2O (▲) and D_2O (■) and VDP-PNIPAM in H_2O (◆) and D_2O (★), respectively.

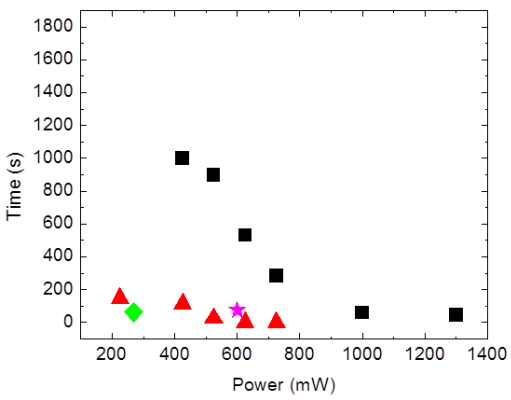

Figure 3.3 Phase transition time change upon laser power. The symbols show PNIPAM in H_2O (▲) and D_2O (■) and VDP-PNIPAM in H_2O (◆) and D_2O (★), respectively.

Table 3.1 Phase transition time and particle size in H_2O and D_2O solution.

Power (mW)		225	425	525	625	725	1000	1300
Time (s)	H_2O	148.0	116.0	26.5	0.0	0.0	NA[**1]	NA[**1]
	D_2O	NA[**2]	1000.0	898.0	529.0	283.0	60.0	45.0
Size (m)	H_2O	3.3	5.3	5.5	11.6	14.1	NA[**1]	NA[**1]
	D_2O	NA[**2]	5.5	6.4	6.7	6.8	9.5	9.1

NA[**1]: Data not available, NA[**2]: Did not show phase transition.

Different solvent shows obvious difference on particle size, particle formation time and threshold power density of phase transition. In H_2O solution, the trapping power threshold to observe phase transition is lower than that in D_2O solution. The phase transition time is also shorter than that in D_2O solution. At the same trapping power, the particle is larger than that in D_2O solution. It is interpreted due to a generated heat in H_2O is more than that in D_2O. The heat caused by the vibronic absorption at NIR region in H_2O solution is larger than in D_2O solution.

Ito et al. reported that 1 W of 1064 nm laser focusing to H_2O and D_2O induces about 22 and 2.6˚C temperature elevation, respectively.[44] The temperature elevation in D_2O solution is quite small compare with in H_2O solution. Therefore phase transition in H_2O occurred more efficiently.

In contrast to in H_2O solution, temperature elevation is almost 1/10 in D_2O. All the experiments were done at room temperature (~25˚C) and solution temperature cannot reach LCST (~32˚C), even we focus 1 W of trapping laser. However we

experimentally observed microparticle formation due to the phase transition. As well as the observation in previous case, phase transition in D_2O suggests molecular assembly formation of PNIPAM due to not only temperature elevation but exerted photon pressure. However we should avoid ambiguity of undesirable heat generation during laser focusing to the solution.

3.2 Heating effect of glass substrate

We are interested in the molecular assembling and phase transition which induced by photon pressure. Therefore it should be better to suppress temperature elevation and/or generation during trapping laser irradiation. It is suggested that NIR laser absorption by glass substrate will generate a heat and elevate temperature.[44]

To clarify temperature elevation due to trapping laser absorption by substrate, we examined glass and quartz which does not absorb NIR light and compared by observing phase transition behavior. Laser focus point was fixed to 10 μm bellow of upper substrate of the chamber.

Figure 3.4 shows the formed phase transition microparticle both glass and quartz sample chamber. PNIPAM/H_2O solution was used and laser power was higher than 525 mW. In both substrates, particle size became larger with increasing the laser power. As we can see in Figure 3.5a, the particle size formed in each sample chamber,

glass substrate cases showed larger particle in all examined laser power range. It implies that glass substrate generate more heat than quartz due to the absorption of trapping NIR laser light.

Although phase transition times were almost similar both glass and quartz substrate above 600 mW, it shows slight difference at 525 mW (Figure 3.5b). More detailed examination of power dependency between 450 to 525 mW range (Figure 3.6) showed clearly longer phase transition time for quartz substrate.

As well as in H_2O, glass substrate showed faster phase transition, larger particle size, and additionally, lower power threshold of phase transition in case of D_2O solution as seen in Figs. 3.7a and 3.7b. Threshold of phase transition with glass substrate, 0.7 W, was much lower than that for quartz substrate at 1.1 W.

The values of phase transition time and particle size on glass and quartz substrates induced in H_2O and D_2O are summarized in Table 3.2 and 3.3, respectively. A heating effect on glass substrate has obviously indicated by these results.

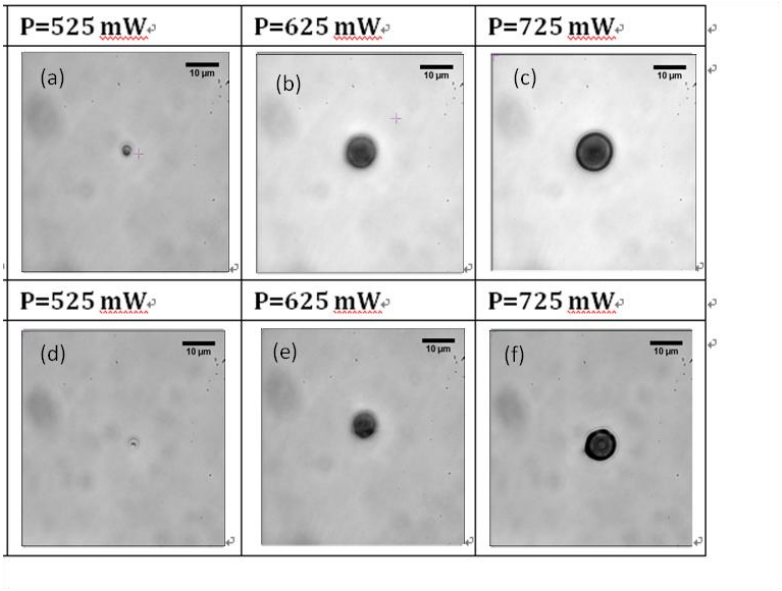

Figure 3.4 Phase transition-induced microparticle formation in H_2O with (a) ~ (c) glass substrate and (d) ~ (f) quartz substrate at each trapping

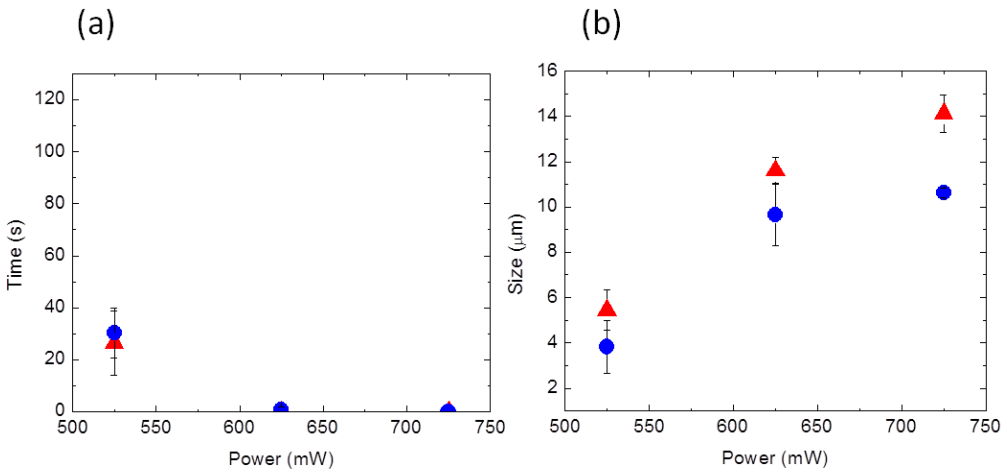

Figure 3.5 Power dependence of (a) particle size and (b) phase transition time in H_2O solution. The symbols show glass (▲) and quartz (●).

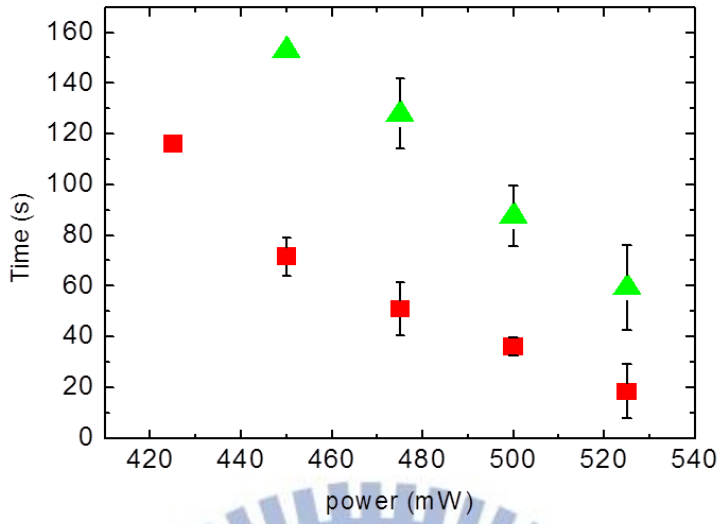

Figure 3.6 Power dependence of phase transition time in H_2O solution with glass (■) and quartz (▲) substrate.

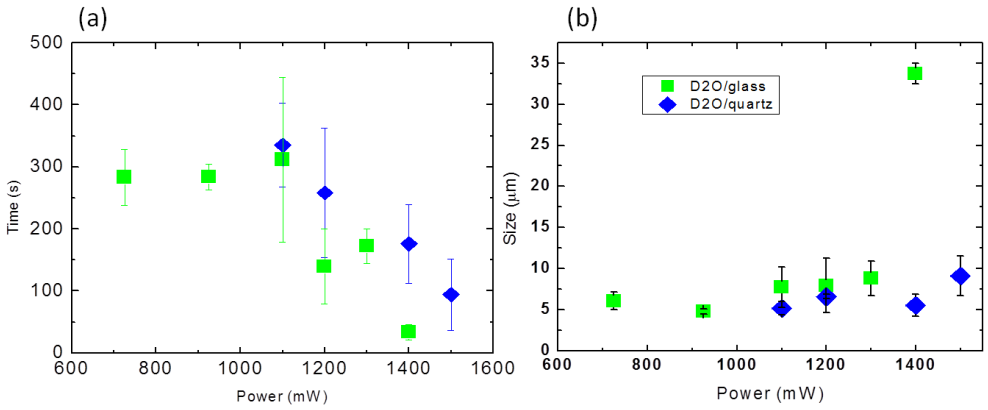

Figure 3.7 Power dependence of (a) phase transition time and (b) particle size formed in the glass (■) and quartz (◆) chamber. PNIPAM/D_2O solution was used.

Table 3.2 The PNIPAM phase transition time and size at each trapping laser power in H_2O solution

Power (mW)		425	450	475	500	525	625	725
glass	Time (s)	116±0.1	71.7±7.5	51±10.5	36±3.6	18.3±10.7	<0.5	<0.5
	Size (μm)	4.4±0.2	4.2±0.3	4.4±0.3	4±0.5	4.2±0.15	11.6±0.6	14.1±0.8
quartz	Time (s)		153±0.1	128±13.7	87.7±12.1	59.3±16.87	<0.5	<0.5
	Size (μm)		4.2±0.1	3.8±0.6	4.1±0.2	4±0.1	9.7±1.3	10.6±0.2

Table 3.3 The PNIPAM phase transition time and size at each trapping laser power in D_2O solution

Power (mW)		725	925	1100	1200	1300	1400	1500
glass	Time (s)	283.0±45.3	283.5±20.5	311.7±133.3	139.3±60.5	172.5±27.8	33.5±12	
	Size (μm)	6.1±1.1	4.8±0.3	7.7±2.5	7.9±3.4	8.8±2.1	33.7±1.3	
quartz	Time (s)			335.0±67.4	258.3±104.6		176.0±63.6	94.0±57.5
	Size (μm)			5.1±0.8	6.6±0.3		5.6±1.3	9.1±2.4

3.3 Position dependence of PNIPAM phase transition

Consider with the heating effect of substrate, we need to compare the phase transition behavior at different height in the chamber. When trapping laser was focused at the middle of the chamber where is far away from the substrate and will have less heating effect from the substrate. We also check the position dependence with glass and quartz substrate. PNIPAM/H_2O solution was used. Laser powers at 450 and 550 mW for glass and quartz substrate were used, respectively. Trapping laser power was decided to form similar size of microparticle in both substrate cases. Results of position dependence experiment for different substrate are summarized in

Figure 3.8. The values of phase transition time and particle size at the different focusing position in the sample chamber for glass and quartz are summarized in Table 3.4, respectively. When the focusing position is far from the substrate more than 10 μm, we can see stable microparticle formation with similar particle size and less size fluctuation. This tendency is more obvious in quartz substrate case. It suggests that the heating effect due to NIR absorption by substrate can be suppressed by using quartz as substrate. Hereafter, we use quartz instead of glass for chamber fabrication aiming to achieve and observe more stable phase transition behavior.

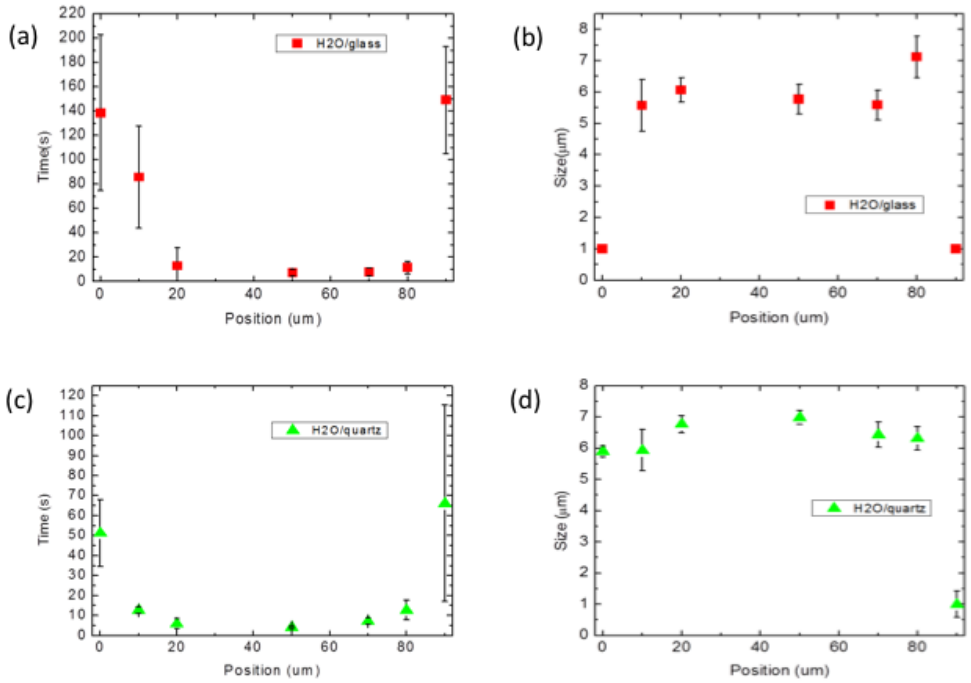

Figure 3.8 Position dependence of (a) phase transition time and (b) particle size with glass substrate(■), and (c) phase transition time and (d) particle size with quartz (▲) substrate. PNIPAM/H_2O solution was used. Trapping laser powers for glass and quartz were 425 and 525 mW, respectively.

Table 3.4 Phase transition time and size at different position of the sample chamber.

Position (μm)		0	10	20	50	70	80	90
glass	Time (s)	138.6±64.1	85.7±41.8	12.9±14.6	7.4±2.7	7.7±3.3	11.4±5.1	149.0±43.9
	Size (μ m)	1.0±0.1	5.6±0.8	6.1±0.4	5.8±0.5	5.6±0.5	7.1±0.7	1.0±0.1
quartz	Time (s)	51.4±16.7	12.7±1.6	5.8±2.5	4.1±0.5	7.1±1.6	12.8±5.1	66.2±49.0
	Size (μ m)	5.4±0.5	5.1±0.4	5.4±0.4	5.8±0.2	5.7±0.2	5.7±0.2	0.7±0.1

3.4 Summary

In this chapter, we examined microparticle formation of PNIPAM at the focal spot of trapping laser both in H_2O and D_2O. Phase transition in D_2O suggests that the particle formation is driven not only by thermal effect but also photon pressure of trapping laser since temperature elevation is not enough to overcome LCST for phase transition of PNIPAM.

We also discussed about the heating effect due to trapping laser absorption by solvent and substrate. The heating effect from the substrate can be identified by changing the substrate from glass to quartz which do not absorb NIR light. The quartz substrate showed higher trapping power threshold and longer phase transition time compared with glass substrate case. This clearly indicates that we can suppress temperature elevation and heating effect by using quartz as substrate. Position

dependence of phase transition implies when the trapping position is far more than 10 μm from the substrate, we can induce rather stable phase transition without particle size fluctuation. Hereafter, we will use quartz as substrate to prevent heating effect of the substrate.

4. Fluorescence lifetime measurement and construction of fluorescence lifetime imaging microscopy (FLIM) system

Steady-state and time-resolved fluorescence spectroscopy have been powerful tool for molecular spectroscopic investigation of fluorescent molecules in condensed phase. During a couple of decades it has grown dramatically due to the development of new optics, detectors, methods, and combing with different measurement systems such as microscopy, and we can detect very tiny signal from a single molecule. Fluorescence spectroscopy and time-resolve fluorescence measurement have already been very useful tool for the imaging of molecular dynamics in chemical, physical, and biological systems with a sensitivity at single-molecule level. Fluorescence technique is used in so many applications: two-photon excited fluorescence (TPEF), fluorescence correlation spectroscopy (FCS) and so on. By introducing and combining with these techniques, fluorescence measurements can provide further information on a wide range of molecular process, such as intramolecular interaction, rotational diffusion, conformation changes, and binding interaction in biological systems.

4.1 Fluorescence from molecule.

There are two very important characters of fluorophore, lifetime and quantum yield. Figure 4.1 shows Jablonski diagram which explains photo-induced activation/deactivation pathways after an excitation of fluorescent molecules. Fluorescence quantum yield and lifetime can be explained along with the rate constants indicated in Figure 4.1. Fluorescence quantum yield is defined by the percentage of emitting photons relative to absorbed photons as explained with eq. 4.1,

$$Q = \frac{k_r}{k_r + k_{ic} + k_{isc}} \dots\dots\dots 4.1$$

where kr, kic, kisc are radiative rate constant, rate constant of internal conversion and intersystem crossing, respectively.

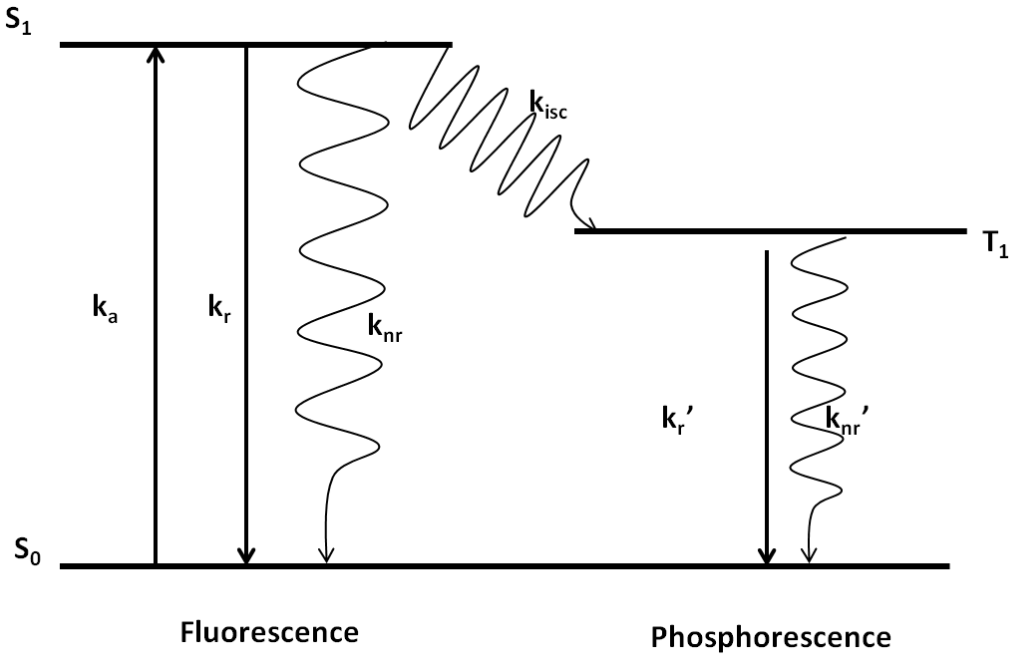

Figure 4.1 Jablonski diagram. S_0 and S_1 are ground and lowest excited singlet state, respectively. T_1 is lowest excited triplet state. The k means rate constant for k_a: absorption; k_r: fluorescence k_r': phosphorescence, k_{nr}, k_{nr}': non-radiative deactivation, k_{isc}-: intersystem crossing

Based on above diagram, the rate equation of fluorescence from S1 state is explained with eq. 4.2;

$$\frac{d(S_1)}{dt} = -k_{S_1}(S_1) = -(k_r + k_{ic} + k_{isc})(S_1) \ldots..4.2$$

By taking an integration of eq. 4.2, we obtain eq. 4.3

$$(S_1) = (S_1)_0 e^{-k_{s_1} t} \ldots \ldots \ldots 4.3$$

The $(S_1)_0$ means the concentration of S_1 state at the initial condition, as it to say instantly after photo excitation. Because emission light intensity is proportional to the concentration of the molecules in S_1 state, it can be presented by following equations,

$$I_{S_1} = I^0_{S_1} e^{-k_s t} = I^0_{S_1} e^{-t/\tau_f} \ldots\ldots\ldots 4.4$$

$$\tau_f = \frac{1}{k_s} = \frac{1}{k_r + k_{ic} + k_{isc}} \ldots\ldots\ldots 4.5$$

Usually, τ_f is called lifetime of S_1.

The lifetime means the average time of fluorophore remains in the excited state after the excitation. Lifetime is sensitive to the interaction between fluorophore and its environment, thus we can obtain environmental information not only from spectral change but also lifetime change.

4.2 Time-correlated single photon counting

For measuring lifetime of fluorescent molecules, there are two typical methods; time domain and frequency domain method. Here we will introduce only time domain method since we use this method for lifetime measurement in this study. For time domain measurement, problems are (1) it is hard to obtain data with ordinary electronic transient recorders and (2) fluorescence signal is usually too weak to make a decay curve. The most popular approach to solve the problem is using "Time-Correlated Single Photon Counting" (TCSPC) method. Equation 4.4 depicts how we can obtain the lifetime of fluorophore by mathematical calculation based on the transitions in Jablonski diagram. By taking the log of integration of eq. 4.2 we

obtain following equation (for single exponential decay)

$$\ln I_{S_1} = \frac{-t}{\tau_f} \ln I^0_{S_1} \quad \ldots\ldots\ldots 4.6$$

The lifetime can be found as a slope of decay curve. For multi-exponential decay, the intensity of fluorescence can be written as eq. 4.7 by introducing additional decay components,

$$I_{S_1} = A_1 e^{-t/\tau_1} + A_2 e^{-t/\tau_2} + \cdots \quad \ldots\ldots\ldots 4.7$$

Figure 4.2a shows schematic drawing how emitted photon from excited molecule will be tagged to construct fluorescence decay curve. Here we decide signal arriving time of excitation light as time t=0. As shown in Figure 4.2a observing timing of emitted photon from excited fluorophore vary depending upon excitation event. Therefore we can record photon observing time as a function of the difference between excitation light arriving time and fluorescence photon arriving time as depicted in the figure such as Δt_1, Δt_2, … . Intensity decay with delay time after the excitation pulse laser coming can be constructed by taking a histogram of arriving photons which becomes as the blue line in Figure 4.2b which can be described as eq. 4.7. From the intensity decay curve, we can calculate lifetime of sample. TCSPC method is base on the highly repetitive single photon counting. As shown in Figure 4.2, photon will be tagged at the time depending upon the delay (i.e. the difference of

the arrival time between excitation pulse and emitted photon from the molecule) after excitation pulse coming. With TCSPC method, it will count just the first photon coming after excitation pulse. Then the time of photon coming will be store in a phton counting module with time-correlated histogram. By using high repetition rate pulse laser as excitation light source, this graph can be taken efficiently by doing this process repeatedly in a short time. The typical result is a histogram with an exponential decay towards later times as shown in Figure 4.2b (lower panel).

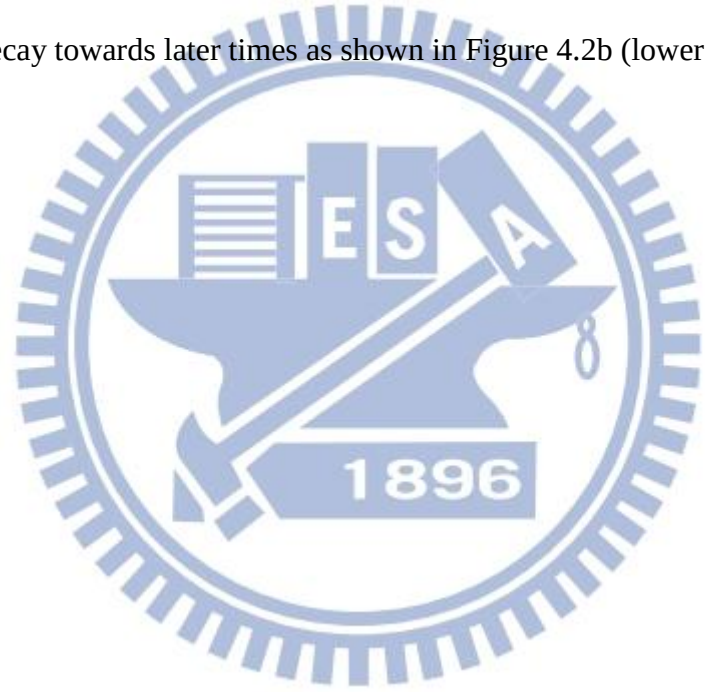

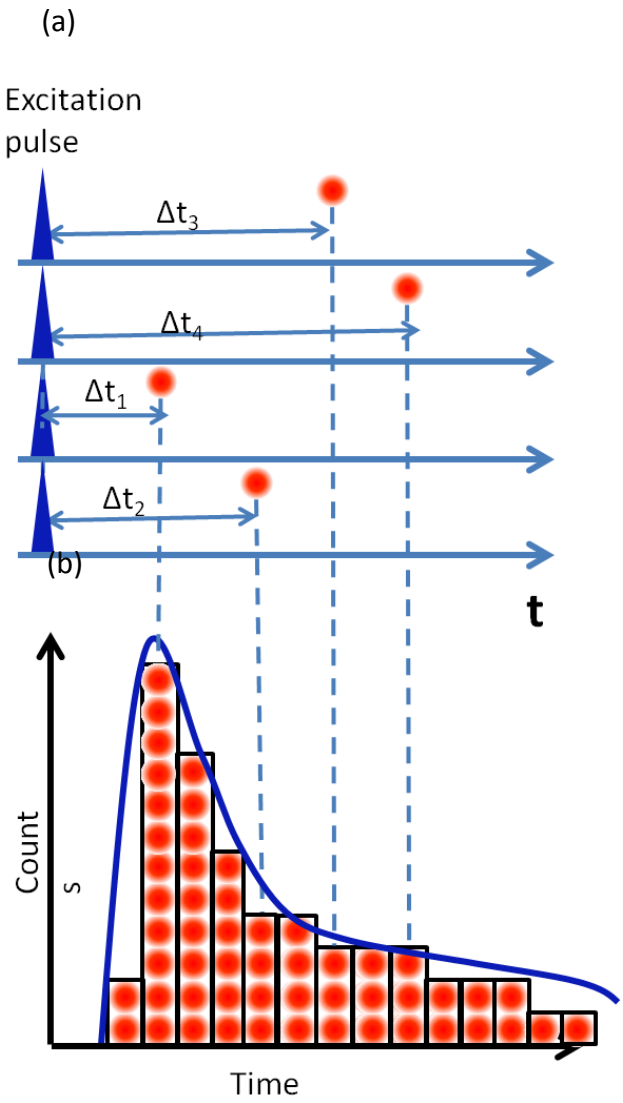

Figure 4.2 Principle of TCSPC. (a) Variation of an arriving time of emitted photon from fluorophore and (b) a histogram constructed from the photons came after the excitation pulse. This histogram is fluorescence decay curve.

This method requires that we need to restrict the photon number to be less than one for each cycle to guarantee that the histogram of photon arrivals would obtained from a single shot time-resolved analog recording. Because the detector and electronics have a dead time, if plural number of photons in one excitation are emitted,

the system would very frequently register the first photon and then missing the following ones: this is called as pulse pile-up. To avoid this problem, the average counts rate at detector should be at most 1~5% of the excitation photon rate. For example, if the excitation laser pulse repetition rate is 80MHz, the average detector count rate should not exceed 4MHz. However, we need to consider the high count rate to make decay histogram quickly, especially for dynamics of lifetime change and fast molecule transition studies. When planning the experiment, we should consider these points and try to find the optimized condition.

Combining the decay curve with eqs. 4.6 and 4.7, we can obtain lifetime information of the molecule. For measuring decay time of intensity, we need specialized electronics to measure the time delay between excitation and emission. The electronics setup is as shown in Figure 4.3. The synchronous signal come from excitation light source is brought to a time-to-amplitude converter (TAC), which generate voltage signal that increases linearly with time, to be the start point to calculate time delay. The detection signal will be sent to a constant function discriminator (CFD), which will accurately calculate the arriving time of pulse, and then its signal is sent to TAC to be stop signal. From the voltage of TAC, we can determine the delay time between excitation pulse and emission from the molecule. Then the voltage information will be converted to digital signal by an

analog-to-digital converter, then sent to computer. The histogram will be composed by repeating this process a lot of times by using high repetition rate pulse light source.

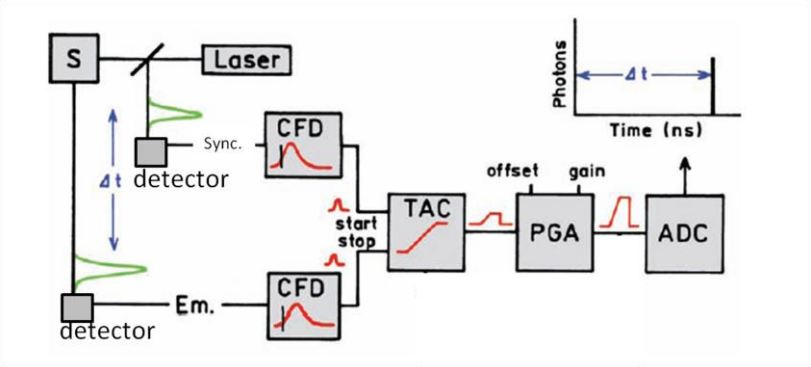

Figure 4.3 Schematic diagram of TCSPC system. From [45]

In TCSPC, one more important point is synchronization signal which is used to be start (or stop) signal of single photon counting. For precise measurement, it needs a very stable synchronization signal source which is surely in phase with the optical pulses. The “stable” means constant peak height and shape. The other requirement of synchronization signal is its steep fall. A good synchronization signal should be as sharp as possible for its trailing edge and without fluctuating baseline value.

4.3 Fluorescence lifetime imaging microscopy (FLIM)

Combing the lifetime measurement with laser scanning microscopy technique, we can use a very powerful method, fluorescence lifetime imaging microscopy (FLIM). Recently, FLIM has been popular for wide range of biological science. For general fluorescence microscopy image, it usually uses fluorescence intensity to construct the image. However fluorescence intensity itself cannot be used to elucidate molecular environment or existence of different fluorophore which emits at similar wavelength. If we just measure the intensity, it is difficult to determine the local environment of molecule.

On the other hand, fluorescence lifetime is independent to concentration, so it can provide more quantitative and accurate information since different molecules usually display different lifetime and we can specify by taking fluorescence lifetime image even in complex mixture of molecular species. The concept of FLIM is shown in Figure 4.4. As we described and shown in the image, fluorescence intensity image cannot distinguish the environmental difference due to plural unknown coefficients. However, the lifetime of different environment/molecule is totally different and can be used to identify the difference of existing molecular species/environment as depicted in the figure. Therefore, FLIM is very powerful tool for quantitative measurement of

the dynamics of molecules in complex environment and structural for microscopic sample.

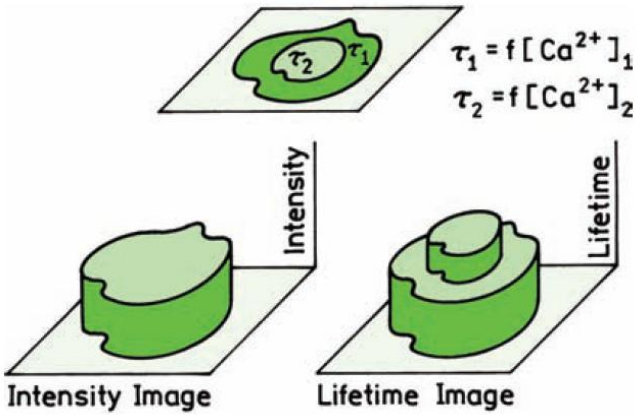

Figure 4.4 Conceptual drawing showing difference of intensity imaging (left) and lifetime imaging (FLIM, right). of FLIM. From [46]

4.4 Evaluation of Fluorescence lifetime imaging microscopy system

As we described in experimental section, we constructed FLIM system. Here we checked spatial resolution of our FLIM system by measuring reference sample.

For the evaluation of spatial resolution of the system, we use fluorescent dye-doped polystyrene (PS) beads. To perform FLIM observation of small specimens with single molecule level sensitivity and resolution, we should have high wavelength resolution not only spatial resolution. Thus we used not only different size of PS beads but also different dye-doped beads since these emit at the different peak wavelength. Fluoresce

beads we used in the series of experiments are listed in Table 4.1. Original sample solution was diluted by purified water and spin-coated on cleaned glass substrate and dried. Prepared spin-coated dye-doped PS samples were used for the FLIM observation.

Table 4.1 The fluorescence beads list.

Ex No.,	Serial No.	Size (μm)	Excitation wavelength (nm)	Emission wavelength (nm)	Concentration in solution (%)	company
1	07310-15	1.0			3.0	polyscience
2	T8880	1.0	488	560	2.0	Invitrogen
3	T8864	0.04	488	560	2.0	Invitrogen
4	17154-10	1.0	441	586	2.5	polyscience
5	17151-10	0.2	441	586	2.5	polyscience

Dye-doped PS beads on the glass substrate was excited by 400 nm light of the SHG of Ti:Sapphire laser which brought to microscope and focued to the sample through the microscope objective lens. Fluorescence signal was corrected by the same objective and brought to APD and decay profiles and fluorescence image were constructed from corrected data by PicoHarp 300 and SymphoTime software as described in chapter 2. A bright-field image of deposited PS beads were measure by CCD camera.

First we performed imaging of the mixture of beads number 1, 2 and 5 where the size of the particles are the same but they are doped different dye (#01 is non-doped,

i.e. non-fluorescent). Mixture of beads was spin coated with adding a surfactant to the solution to obtain good monolayer film of PS beads [47]. A bright field image of fabricated PS beads monolayer film is depicted in Figure 4.5 (a) and we cannot distinguish the difference of the beads. PS beads were excited by 400 nm laser light and correct all the fluorescence without using monochromator. Figure 4.5b and 4.5c shows fluorescence intensity image (5b) and fluorescence lifetime image (5c), respectively. In the intensity image we can see the intensity difference depend on the position in the image; near the center of the image we find intense spot and weaker spots at the right and right-top side of the intense spot. Additionally, even the position the particle exist in the bright field image did not necessarily show the fluorescence. These particles are corresponding to non-doped PS beads. Although we can recognize the difference of dye-doped or non-doped, it is still difficult to distinguish the difference of fluorescent particles from the intensity image. In contrast, we can see the sharp difference in lifetime image as depicted in Figure 4.5 (c). Intense spot in the intensity image shows longer fluorescence lifetime and weaker spots shows shorter lifetime.

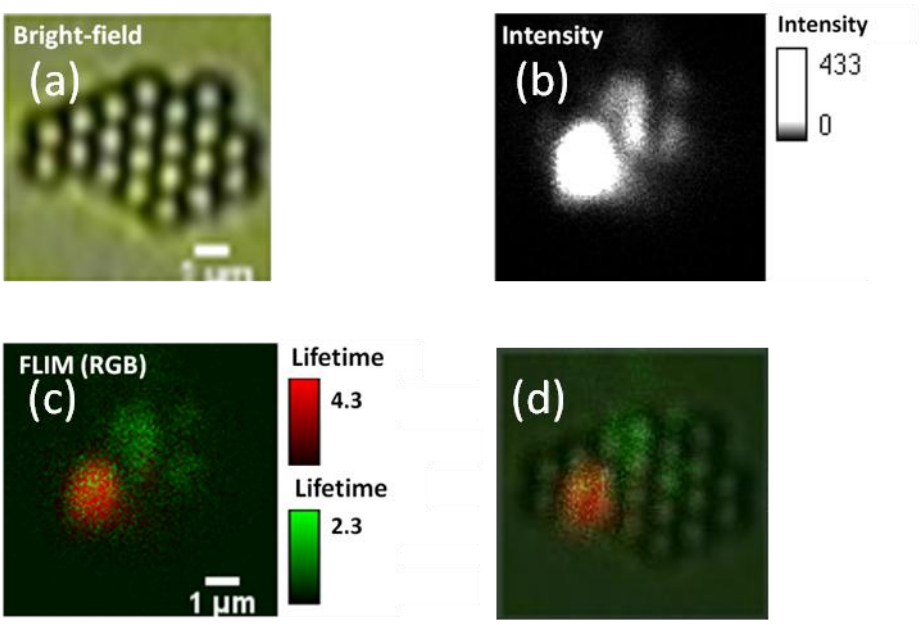

Figure 4.5 Pictures of mixed PS beads monolayer on the grass observed by (a) bright-field, (b) fluorescence intensity, (c) fluorescence lifetime, and (d) superimposed image of (a) and (c). The lifetimes of ~4 ns (red) and ~2 ns (green) correspond to the fluorescence lifetime of No.2 and No. 4, respectively. A 40x long working distance objective lens was used for both bright field and FLIM images..

Fluorescence lifetime value obtained from the decay curved measured at each pixels for red and green areas in Figure 4.5 (c) are 3.85 ns and 0.034 ns for two exponential and 2.27 ns with single exponential fitting, respectively. We have measured fluorescence lifetime of beads No. 2 and No. 4 in bulk solution and obtained their lifetime as 4.05 and 1.19 ns (No. 2, 4.05 ns lifetime is minor component less than 30%) and 2.43 ns (No. 4), respectively. Therefore, observed longer lifetime in the strong emission region is considered to No. 2 and shorter one is No. 4. Here short lifetime component of No. 2 showed disagreement with the lifetime observed in the bulk solution. It can be interpreted due to low signal to noise (S/N) ratio in FLIM

measurement. For FLIM measurements, the accumulation time for each pixel is far shorter compared to that in bulk measurements. Thus, S/N ratio becomes worth and difficult to observe negligible lifetime component. Although negligible component detection was difficult compared to bulk fluorescence lifetime measurement, we succeeded to recognize different fluorescent lifetime component with sub ns time resolution.

Spatial resolution of FLIM system, is determined by the focused laser spot size since the spot size cannot be infinity small due to the diffraction limit of the light. Therefore observable fluorescence spot size in fluorescence image reflects the laser spot size when fluorescent object is far smaller than that of excitation light; it means we need to use quite small fluorescent object to determine spatial resolution of our FLIM system and under such circumstance observed fluorescence spot size corresponds to the size of laser spot as depicted in Figure 4.6. In spatial resolution determination, we used high NA oil-immersion objective lens (NA=1.3) and excitation wavelength was 400 nm from the SHG of Ti:S laser. Therefore theoretical diffraction limited spot size of excitation laser light is calculated to 180 nm by using following equation,

$$r_0 = \left(\frac{(r^2 \times f^2)}{{Z_R}^2}\right) \div \left(1 + \left(\frac{f}{{Z_R}^2}\right)^2\right) \ldots\ldots\ldots\ldots\ldots 4.8$$

where r_0 is beam waist size, M is M-square factor which express beam propagation

quality, f is focusing length of the lens, n is refractive index of the medium and Z_R is Rayleigh length which is expressed as following;

$$Z_R = \frac{\pi \times r^2 \times n}{M^2 \times \lambda} \ldots\ldots\ldots\ldots\ldots\ldots\ldots 4.9$$

It can be turned into simplified as $r_0=0.61\ \lambda$ /NA.

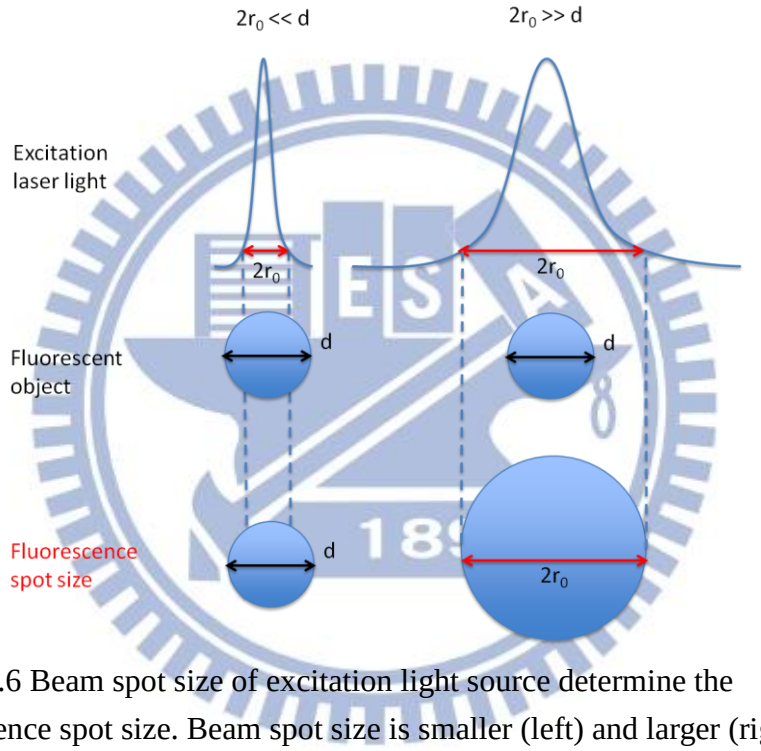

Figure 4.6 Beam spot size of excitation light source determine the fluorescence spot size. Beam spot size is smaller (left) and larger (right) than that of fluorescent object.

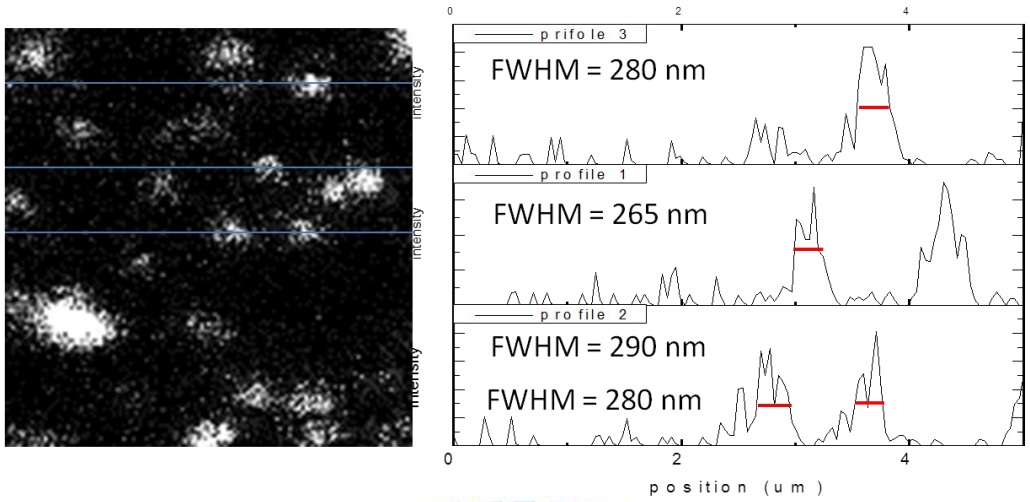

Figure 4.7 Fluorescence intensity image of 40 nm fluorescent beads and cross-sectional line profile along the lines in the image. The picture size is 5x5 μm^2.

Figure 4.7 was obtained by using No. 3 dye-doped PS beads mentioned in Table 4.1 which is 40 nm in diameter. The size of the PS beads is much smaller than that of theoretically calculated diffraction limited beam spot size of 180 nm, and therefore we can assume the observed spot size of fluorescence spot is comparable to the focused beam spot size. The size of PS beads from fluorescence image can be decided by the value of full width at half maximum (FWHM) in cross-sectional analysis done along the lines in the fluorescence image. The mean value of FWHM is obtained as 279 nm i.e. the spatial resolution of our system is determined to ~280 nm.

4.5 Summary

We discussed a construction of fluorescence lifetime image microscopy system. Combining the stage-scanning fluorescence imaging microscopy system and TCSPC system, we can do the lifetime imaging. We determined the spatial resolution of constructed FLIM system as 280 nm by using 40 nm fluorescent beads. This system will be used for the lifetime imaging of fluorescent VDP-PNIPAM sample.

5. Phase transition dynamic of VDP-PNIPAM by fluorescence microscopy

5.1 Laser trapping induce phase transition of VDP-PNIPAM

Figure 5.1 shows a sequential pictures of phase transition process of VDP-PNIPAM under 200 mW trapping laser irradiation in H_2O. By starting the irradiation of the trapping laser, we observed the particle formation as shown in Figure 5.1 after some moment later. In Figure 5.1 case, phase transition was observed around 58 sec after starting laser irradiation and particle slowly enlarged its size by continuous trapping laser irradiation, and the size reached to its maximum. And then, formed particle disappeared quickly when trapping laser irradiation was stopped. VDP-PNIPAM in H_2O shows quite similar phase transition behavior as NIPAM in H_2O such as increasing of maximum particle size depending upon the laser power as shown in Figure 5.2. We can see an enlargement of fluorescent spot with increasing the laser power. A tiny 2~ 3 μm spot at 100 mW of trapping laser became more than 20 μm at 450 mW.

We found that some clear differences between VDP-PNIPM and PNIPAM phase transition behavior: VDP-PNIPM showed shorter phase transition time and lower power threshold for phase transition. Theoretically VDP-PNIPAM should show same

phase transition behavior since polymer backbone structure is the same. However threshold of the phase transition became less than 100 mW in VDP-PNIPAM; meanwhile it was 200 mW in PNIPAM. If trapping power was larger than 200 mW, then phase transition of VDP-PNIPAM occurred immediately. It can be interpreted due to two possible reasons; one is a difference of molecular weight of the molecules, because the average molecular weight of VDP-PNIPAM is larger than that of PNIPAM. It is known that phase transition behavior of polymer depends on the size of the molecule. Thus, we can attribute observed difference on phase transition time and trapping power threshold to the difference of the molecular size. One more possible reason is an excitation light for fluorescence detection. For these experiments, we turn on the excitation and trapping lasers at same time. Light intensity is quite low at the level of mW, however, it can induce more efficient phase transition as we will discuss later.

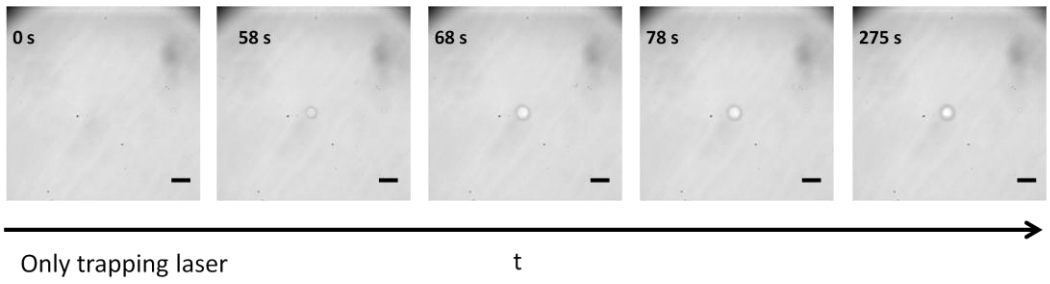

Figure 5.1 Particle formation due to the phase transition of VDP-PNIPAM induced by trapping laser in H_2O solution. Trapping laser power was 200 mW. Scale bar = 10 μm.

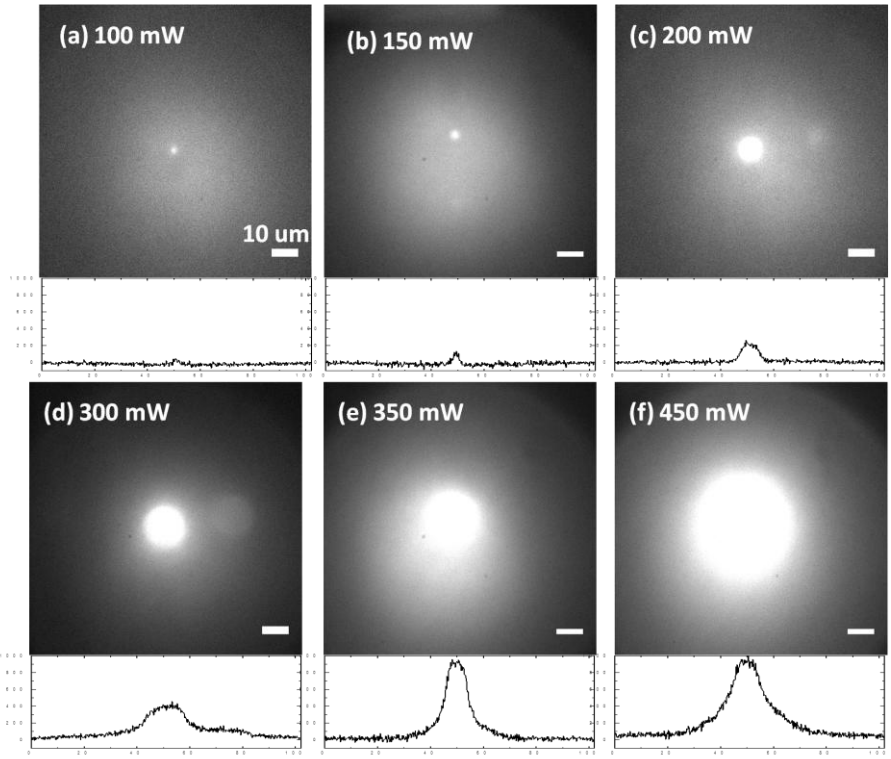

Figure 5.2 Fluorescence images of particle formed by laser trapping. Values in the images indicating trapping laser power used for inducing the phase transition. VDP-PNIPAM was in H_2O. Excitation wavelength was 325 nm.

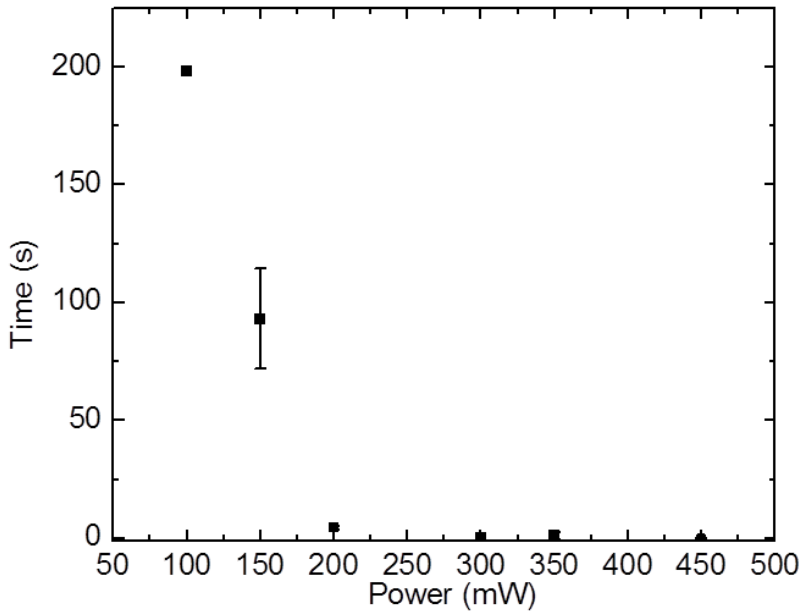

Figure 5.3 Phase transition time change depends on trapping laser power. A 325 nm fluorescence excitation laser was irradiated simultaneously with trapping laser. VDP-PNIPAM was in H_2O solution.

Table.5.1 The VDP-PNIPAM phase transition time each trapping laser power in H_2O solution.

Power (mW)	100	150	200	300	350	400	450
Time(s)	198.0± 0.1	93.0 ± 21.2	4.5± 0.8	0 ± 0.1	1.0 ± 1.7	0 ± 0.1	0 ± 0.1

5.2 Fluorescence decay dynamics of VDP-PNIPAM during phase transition

We used FLIM system for the measurement of fluorescence lifetime of VDP-PNIPAM during phase transition. Here phase transition was induced by 200 mW of trapping laser light to the sample solution. Fluorescence excitation light (375 nm,

12 μW) was also focused to the focus point of trapping laser and corrected the fluorescence from the trapped molecules with the same objective lens. Figure 5.4 shows the fluorescence decay curves of VDP-PNIPAM in water before and during transition, i.e. coil and globule state fluorescence lifetime. An instrument response function (IRF) measured at 375 nm was also shown together. FWHM of IRF is ~150 ps and it is determined as time-resolution of the lifetime measurement system.

As seen in the figure, VDP-PNIPAM showed clear difference of decay profile between before and during phase transition. Fitting of obtained decay curve indicating there are two lifetime components both before and during phase transition. Main longer lifetime component (6.9 ns) before phase transition became 4.2 ns after phase transition. The lifetime components and amplitude (percentage) of each decay components are summarized in Table 5.1. A value of 6.9 ns is similar to the lifetime observed with 9-(p-N,N-dimethylanilino)phenanthrene (9Dphen), which is composed with dimethyle aniline moiety and phenanthrene moiety, corresponds to the VDP moiety of VDP-PNIPAM.[48, 49] Based on time-resolved spectroscopy of 9Dphene, solvent polarity decreasing causes a decrease of fluorescence lifetime. For example 7 ns of fluorescence lifetime in acetonitrile (polarity ~37.5) became short as 2.7 ns in diethyl ether which polarity is ~ 4.3. Therefore observed shortening of the lifetime after phase transition can be interpreted due to the polarity decrease of surrounding

environment of VDP. It is quite reasonable because phase transition of PNIPAM occurred with a dehydration of water and surrounding environment of polymer should be more hydrophobic, i.e. lower polarity.

Another interesting finding from lifetime data is an existence of two decay components in VDP-PNIPAM. Fluorescence lifetime of 9Dphene in bulk solution showed single decay component independent to the solvent. However, VDP attached to the PNIPAM chain showed two decay components. Before phase transition, fluorophore molecules should exist in rather homogeneous environment. However decay analysis suggests fluorophore feels different environments and showed two different lifetime component. Shorter lifetime component with 1.6 ns suggests VDP is exposed to local hydrophobic environment which exists in the polymer/solvent matrix.

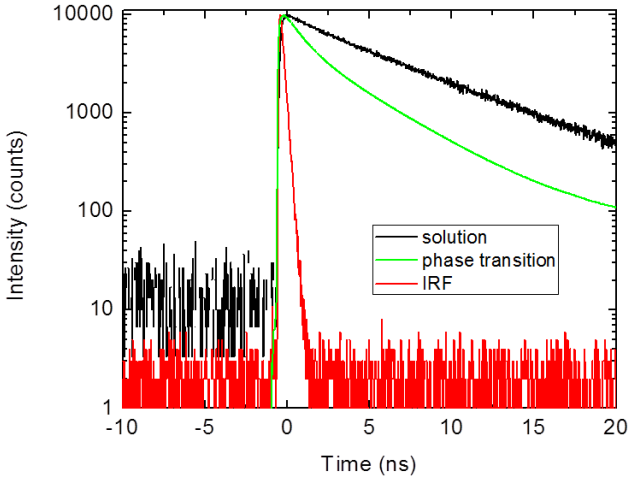

Figure 5.4 Fluorescence decay curve of VDP-PNIPAM in H_2O before (green) and during (black) phase transition. Excitation wavelength and laser power was 375 nm and 12 μW. Trapping laser power was 200 mW.

Table 5.2. Fluorescence lifetime decay parameters of VDP-PNIPAM before (green) and during (black) phase transition.

	Before phase transition	During phase transition
τ_1 (ns)	6.9	4.2
τ_2 (ns)	1.6	1.07
A_1 (%)	80.5	45.6
A_2 (%)	19	54.4

One of the advantage of this experimental setup is that we can measure fluorescence image, spectrum, and fluorescence decay curve at the same time. As shown in the system diagram in chapter 2, emission form the sample is devide into two to measure image and spectrum, and the one of the path will be divided into two again. Although fluorescence signal becomes weaker with this light dividing

procedure, we can obtain sufficient quality of image, spectra and decay data even with weak signal. Thus we tried to measure fluorescence image and decay curve of phase transition simultaneously.

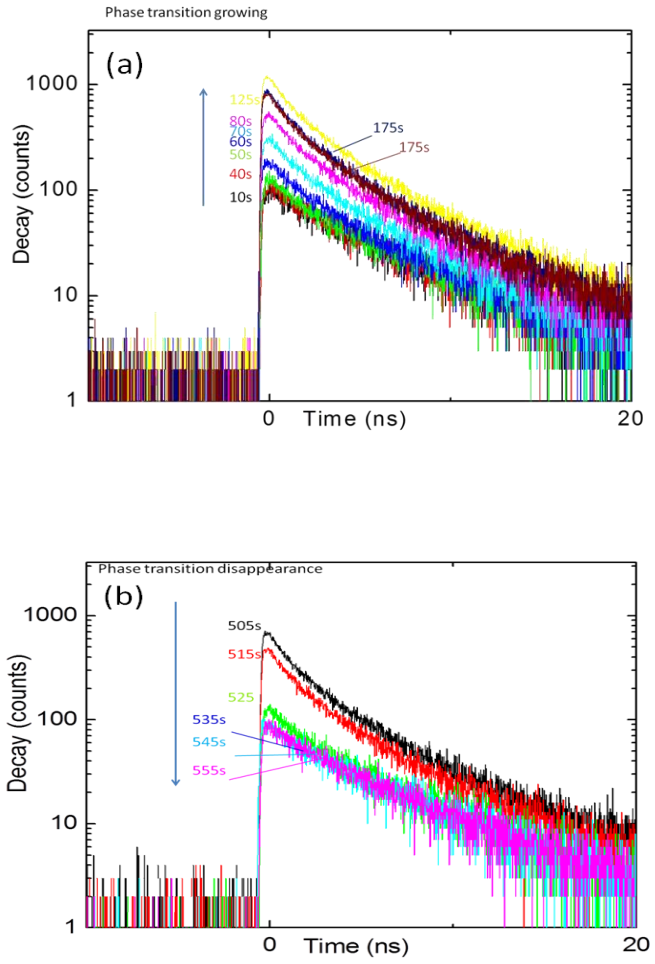

Figure 5.5 Fluorescence decay curves measured during phase transition process at (a) particle formation and (b) particle disappearance. Laser trapping power was 200mW. Fluorescence excitation was at 375 nm with 12 W

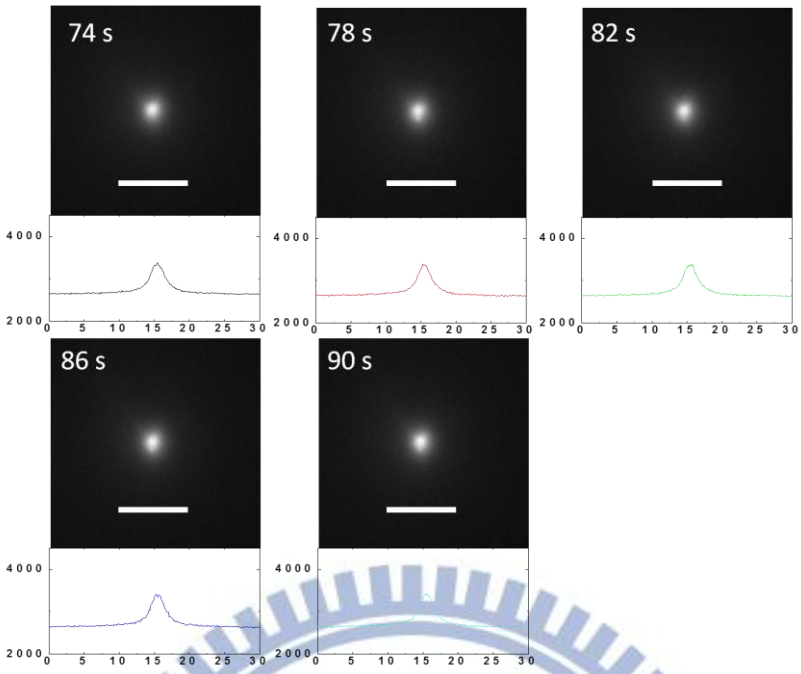

Figure 5.6 Fluorescence images obtained simultaneously with fluorescence decay measurements in particle formation process shown in Figure 5.5a. Laser trapping power was 200mW. Fluorescence excitation was at 375 nm with 12 μW. Scale bar is 10 μm.

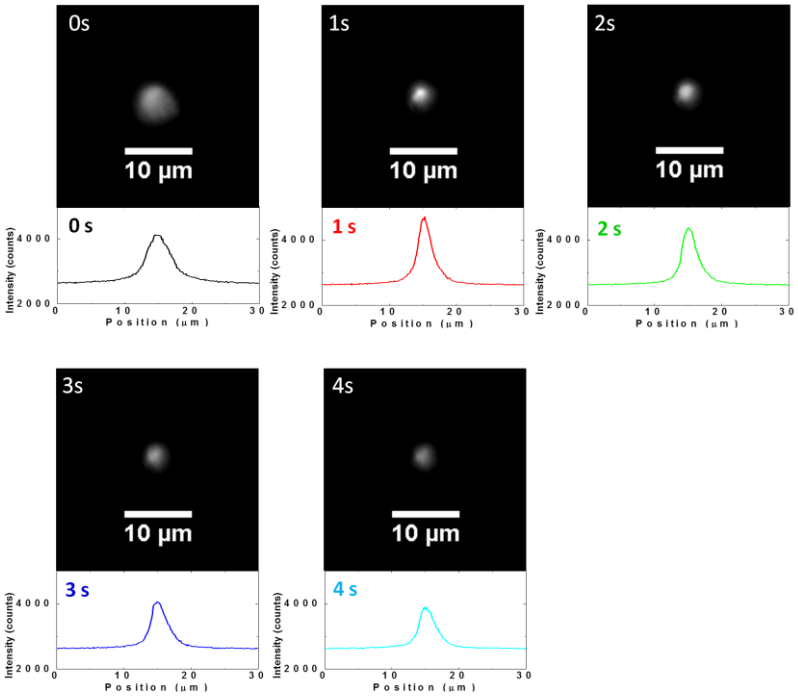

Figure 5.7 Fluorescence images obtained simultaneously with fluorescence decay measurements in particle disappearance process shown in Figure 5.5b. Laser trapping power was 200mW. Fluorescence excitation was at 375 nm with 12 μW. Scale bar is 10 μm.

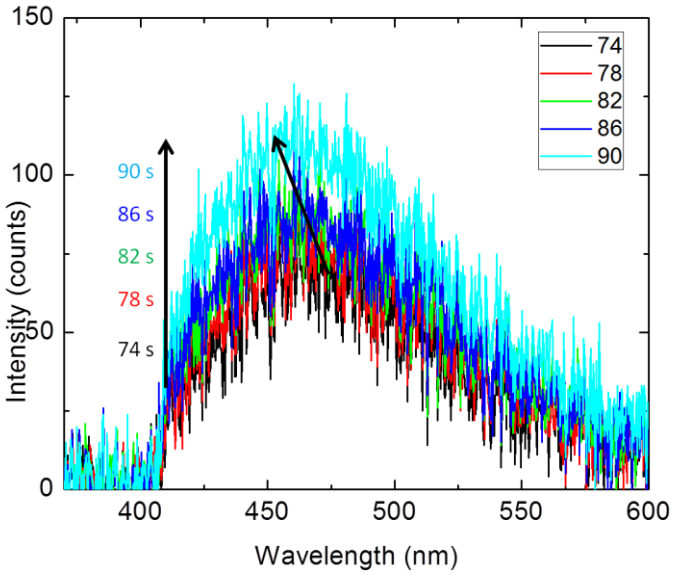

Figure 5.8 Fluorescence spectra measured simultaneously with fluorescence decay measurements in particle formation process shown in Figure 5.5a. The spectrum shifted from 480 nm to 455 nm is seen in the figure. Laser trapping power was 200mW. Fluorescence excitation was at 375 nm with 12 μW.

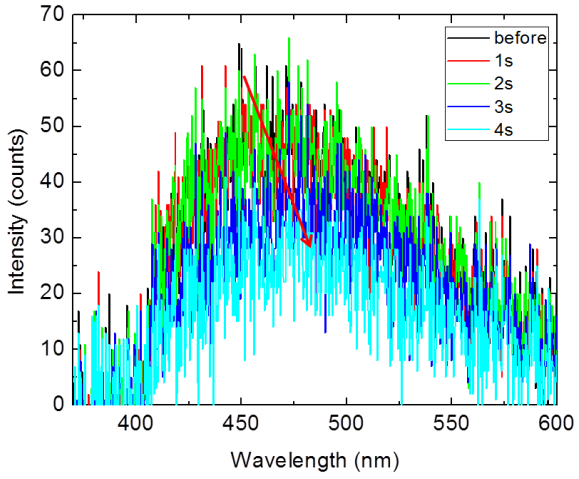

Figure 5.9 Fluorescence spectra measured simultaneously with fluorescence decay measurements in particle disappearance process shown in Figure 5.5b. The spectrum shifted from 450 nm to 480 nm is seen in the figure. Laser trapping power was 200mW. Fluorescence excitation was at 375 nm with 12 μW.

Figure 5.5, 5.6 and 5.7, and 5.8 and 5.9 show simultaneously measured fluorescence decay dynamics, image and spectrum of phase transition process. Phase transition was induced by irradiation of 200 mW trapping laser. Decay curves shown in Figure 5.5 were obtained for 10 s accumulations. Phase transition with particle formation was visualized by temporal decay curve shape change in Figure 5.5, fluorescence intensity increase in fluorescence images in Figure 5.6 and peak wavelength shift from 480 nm to 455 nm in fluorescence spectra. Bathochromic shift of fluorescence spectra during phase transition indicates dehydration in PNIPAM matrix.

When turning off the trapping laser, we can observe reversible phenomena again in the change of fluorescence decays, images, and fluorescence spectra with shifting back to 480 nm in 5 s. The particle formation process, i.e. dehydration process, is relatively slower than the particle disappearance process, i.e. hydration process.

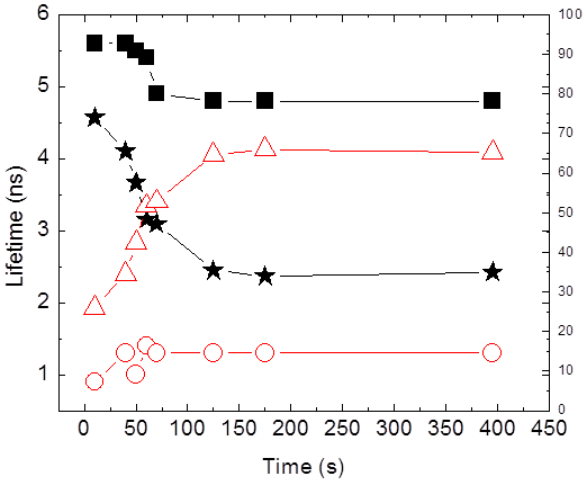

Figure 5.10 Lifetime and amplitude values obtained from the decay curves showed in Figure 5.5a, particle formation process. Vertical line in the graph indicates when phase transition observed. The symbols mean the lifetime (■) and amplitude (★) value for long component and lifetime (○) and amplitude (△) value for short component.

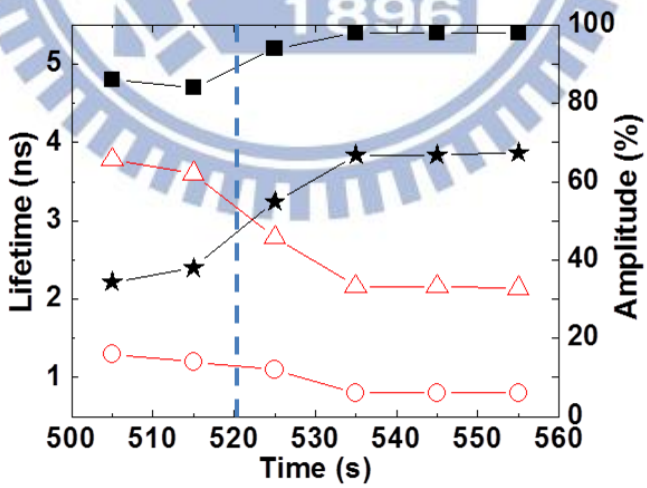

Figure 5.11 Lifetime and amplitude values obtained from the decay curves showed in Figure 5.5a, particle formation process. The symbols mean the lifetime (■) and amplitude (★) value for long component and lifetime (○) and amplitude (△) value for short component.
Vertical line in the graph indicates when trapping laser was turned off.

Combined measurements of fluorescence decay, image and spectrum help us to know all aspects of phase transition information. We can know the lifetime change, spectrum shifted, and images change at the same time. From multimodality of our simultaneous observation tells us when phase transition is started and stopped more clearly than doing single measurements separately.

In actually we have reported slower spectrum shift when we turn off the trapping laser. Peak wavelength of fluorescence spectrum shifted back to original wavelength with ~5 s after turning off the trapping laser. Meanwhile, particle formed by trapping laser disappeared much faster.[50]. We found that long lifetime component were not recovered with in 5 s but it needed more time as shown in Figure 5.5b. This results are consistent with phase transition dynamics observed in transient grating observation.[50] The lifetime measurement gives us more detailed information which spectrum change can not describe.

5.3 Spectra and lifetime change of VDP-PNIPAM phase transition

One of the purpose to use VDP-PNIPAM as a probe molecule of fluorescence measurement is to obtain more information of phase transition dynamics. In previous study[50], the phase transition of VDP-PNIPAM shows blue shifted emission

spectrum. Here, we measured the emission spectrum at different temperature by using heating stage and detect under microscope. Mercury lamp was used as fluorescence excitation light source (excitation wavelength is 325 ~ 375 nm). The sample was placed at the center of the heating stage. We should notice that the temperature of the sample cannot coincide with the value given by temperature controller due to the experimental/equipment problem. Thus we check the difference between displayed value and sample value by checking the fluorescence shift and determined the difference is 2.5~3.0 ˚C.

Figure 5.12 and 5.13 show the fluorescence spectra of VDP-PNIPAM in H_2O and D_2O measured under microscope. These spectra were measured without pinhole, i.e. can be considered as same as bulk fluorescence measurement. The temperature values showed on the graph are display value on the heating plate controller. As we know that the VDP-PNIPAM shows phase transition at 32 ˚C, we can define the phase transition temperature even the value of heating plate controller is incorrect. The spectrum showed the blue shift from 480 to 448 nm when temperature increased. The blue shifted spectrum means the dehydration of polymer chain occurred. Figure 5.14 shows the peak value at each temperature in H_2O and D_2O solutions. The difference of phase transition temperature between H_2O and D_2O solution was 1~2 degree and higher phase transition temperature was observed in D_2O. Observed solvent

dependent phase transition temperature difference suggests different interaction between polymer chain and solvent molecules, i.e. the hydrogen bonding between polymer and solvent are different depending upon the solvent.

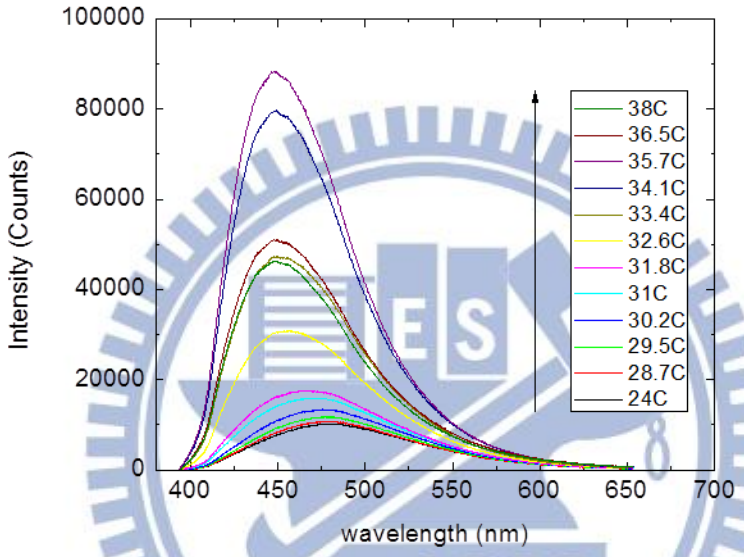

Figure 5.12 Temperature dependence of VDP-PNIPAM spectrum in H_2O solution.

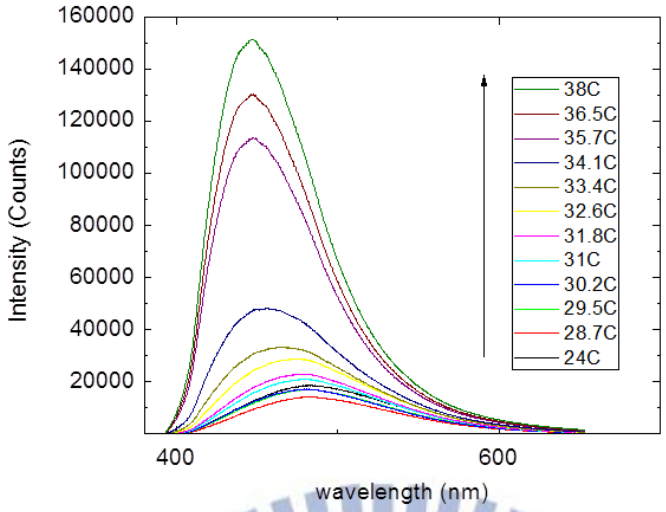

Figure 5.13 Temperature dependence of VDP-PNIPAM spectrum in D_2O solution.

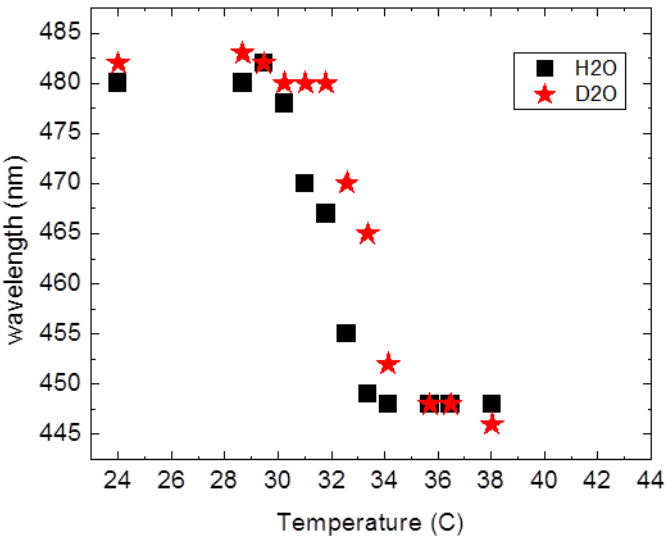

Figure 5.14 Temperature dependent of peak wavelength of spectrum. The horizontal value is compensated temperature.

Table 5.3 Peak wavelength of VDP-PNIPAM at different temperature.
Temperature value are compensated values.

Temperature (˚C)		24	28.7	29.5	30.2	31	31.8
Peak wavelength (nm)	H_2O	480	480	482	478	470	467
Peak wavelength (nm)	D_2O	482	483	482	480	480	480

Temperature (˚C)		32.6	33.4	34.1	35.7	36.5	38
Peak wavelength (nm)	H_2O	455	449	448	448	448	448
Peak wavelength (nm)	D_2O	470	465	452	448	448	446

Combining the microscope with lifetime system, we can measurement spectrum and lifetime decay at the same time. The difference of microscopy setup is that we need to put a confocal pinhole in the optical path to the detector. The other difference is that we introduce pulse 375 nm laser light to the focus point of trapping laser as excitation light. Excitation laser power was 12 μW. Simultaneous lifetime and spectrum measurement results of heat induced phase transition are shown in Figure 5.15~ 5.18.

The spectrum shape is not the same as previous spectrum because we need to put one more dichroic mirror for introducing trapping laser. Those spectrums show a sharp cut at 420 nm which is duo to used long pass filter. The lifetime decay shows in Figure 5.17 and 5.18. By increasing the temperature, the decay became faster. The lifetime obtained from the analysis of decay curves were summarized recorded in Figure 5.19 and 5.20.

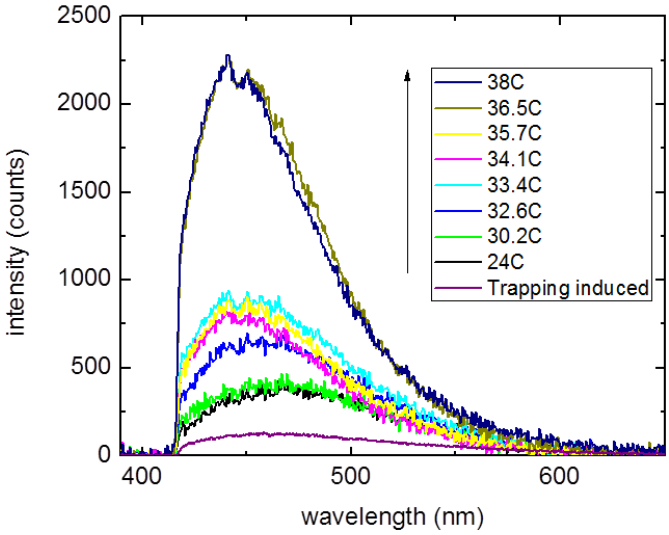

Figure 5.15 Spectrum detected at different temperature in H_2O solution. Excitation was at 375 nm. Spectrum obtained under trapping condition was shown together. Trapping laser power was 200 mW.

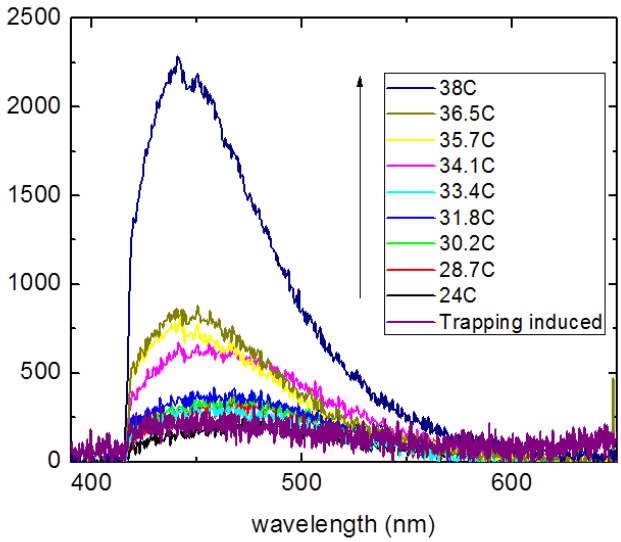

Figure 5.16 Spectrum detected at different temperature in D_2O solution. Excitation was at 375 nm. Spectrum obtained under trapping condition was shown together. Trapping laser power was 200 mW.

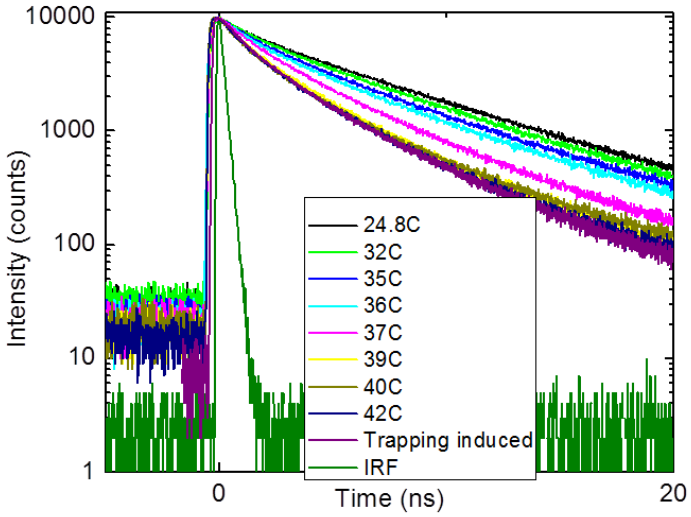

Figure 5.17 Decay curves at different temperature in H_2O solution. Excitation was at 375 nm. Decay obtained under trapping condition was shown together. Trapping laser power was 200 mW.

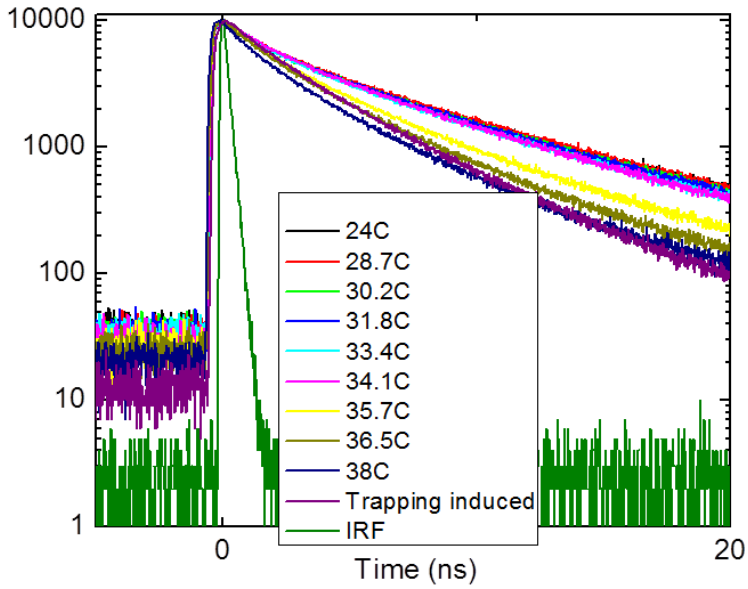

Figure 5.18 Decay curves at different temperature in D_2O solution. Excitation was at 375 nm. Decay obtained under trapping condition was shown together. Trapping laser power was 700 mW.

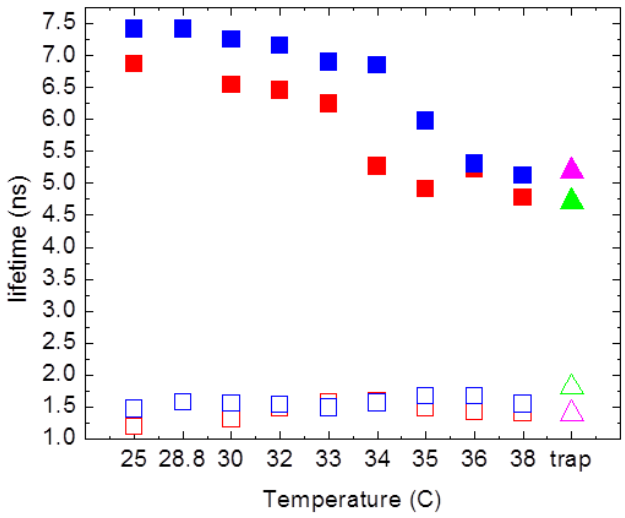

Figure 5.19 Temperature dependent fluorescence lifetime change for H_2O (red, purple) and D_2O (blue, green) shown in Figs. 5.16 and 5.17. Solid and open symbol mean the long and short lifetime values.

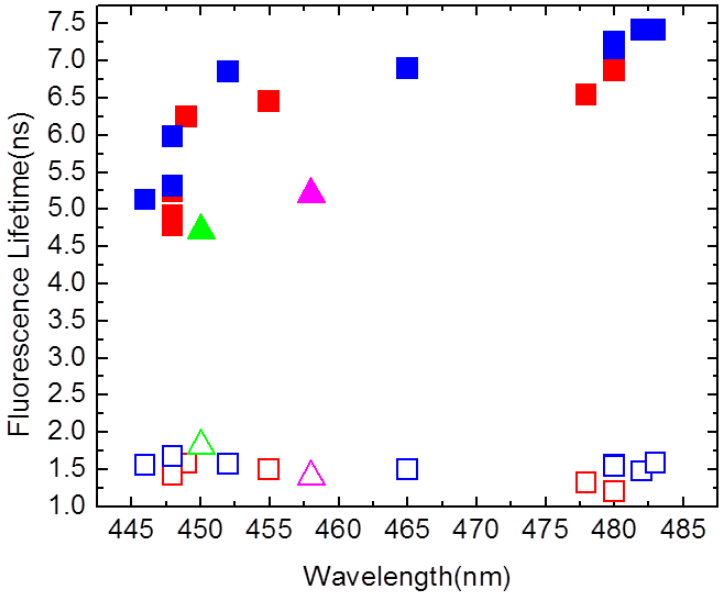

Figure 5.20 Fluorescence lifetime change was plotted against peak wavelength of simultaneously measured fluorescence spectra. All data for H_2O and D_2O are summarized. The symbols mean the same as in Figure 5.18.

Table 5.4. Temperature dependent peak wavelength and lifetime value change.

Temperature (˚C)		24	28.7	30.2	31.8	33.4	34.1	35.7	36.5	38	Trapping
Peak wavelength(nm)	H_2O	480	--	478	455	449	448	448	448	448	458
τ_1		6.9	--	6.5	6.3	6.2	5.3	4.9	5.2	4.8	5.2
τ_2		1.2	--	1.3	1.5	1.6	1.6	1.5	1.4	1.4	1.4
Peak wavelength(nm)	D_2O	482	483	480	--	465	452	448	448	446	450
τ_1		7.4	7.4	7.3	--	6.9	6.8	6	5.3	5.1	4.7
τ_2		1.5	1.6	1.4	--	1.5	1.6	1.7	1.7	1.5	1.8

Figure 5.21 shows that the fitting results of obtained decay curve by using one or two decay component(s) in exponential fitting. From the residual and χ^2 value, we can conclude that the fitting with two decay components is more suitable for the analysis of obtained data than that with one component fitting. So we choose two exponential fitting to fit the decay results showen in Figure 5.17 and 5.18.

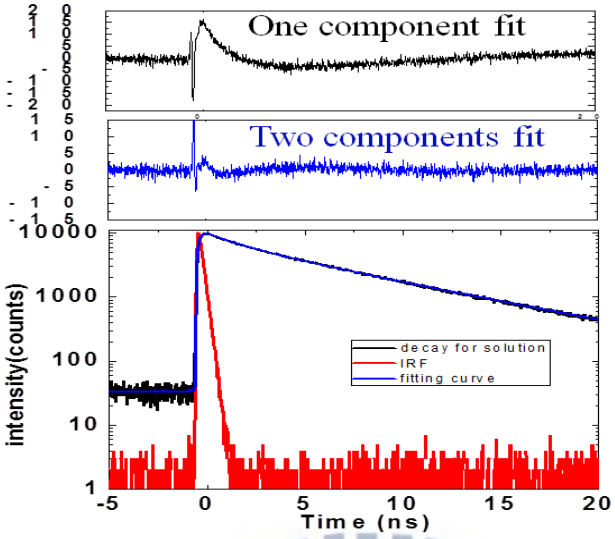

	One component fit	Two components fit
τ_1(ns)	6.4	7.1
τ_2 (ns)		1.8
A_1 (%)	100	66
A_2 (%)		34
χ^2	4.5	1.4

Figure 5.21 The decay curve of VDP-PNIPAM in solution at 25 ˚C fitted by one and two decay components.

Table 5.5 Lifetime components of fitting analysis shown in Fig. 5.24.

	One component fit	Two components fit
τ_1(ns)	6.4	7.1
τ_2 (ns)		1.8
A_1 (%)	100	66
A_2 (%)		34
χ^2	4.5	1.4

5.4 Spatially resolved fluorescence lifetime measurement in phase transition induced microparticle

We showed that fluorescence lifetime before and during phase transition is quite different. In phase transition region, fluorescence decays faster and lifetime becomes shorter than that without phase transition. Then we examine the lifetime measurements at different position of phase transition particle to clarify spatial homogeneity/inhomogeneity in the particle by changing excitation/observation position as shown in Figure 5.22. There are two possible compositions in the particle. One consideration is inhomogeneous composition in the phase transition particle: in this case dehydration degree may be different depend on the distance from the focus point of trapping laser. Another consideration consideration is the composition of phase transition particle in every position can be the same.

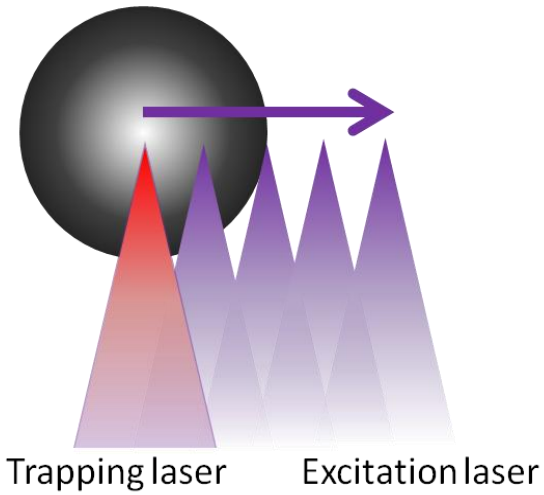

Figure 5.22 Schematic drawing of position dependent lifetime experiment in phase transition particle.

Figure 5.23 shows the positional relationship between particle and fluorescence observation. Cross hair in the images indicates fluorescence measurement point. Figure 5.24 shows fluorescence decay curved observed at the mentioned position in Figure 5.23. In this experiment phase transition particle was formed in H_2O solution by focusing 200 mW of trapping laser and fluorescence decay curves were measured by using 375 nm femtosecond laser (12 μW) as excitation light. Obtained decay curves can be classified into two segments. When the decay was measured in the particle, the lifetime decay are the same and did not show distance dependent change. It was shorter than that measured out of phase transition particle. It means in particle, the dehydration degree of polymer chain does not have obvious difference, but rather homogeneous. When we measured the fluorescence decay at out of particle, decay curves were almost similar as what we observed in bulk solution. Thus we can conclude that outside of the phase transition region even very near of the edge of the particle, which is shown as 5 μm data in the experiment, is same as non-phase transition region in bulk solution. Fluorescence lifetimes at each position were summarized in Table 5.6.

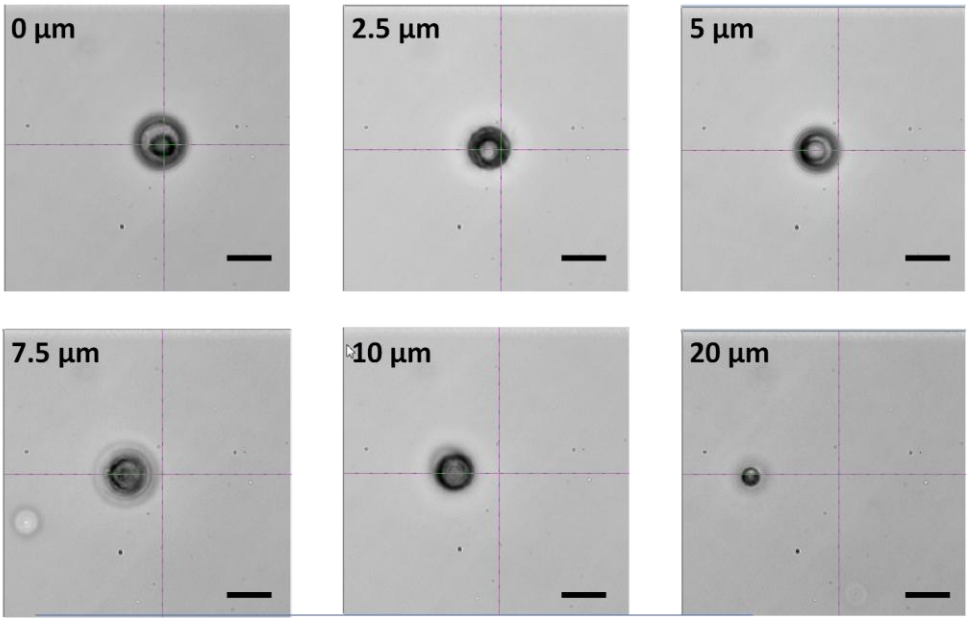

Figure 5.23 The picture of excitation position dependence lifetime measurement in H_2O solution. Scale bar = 10 µm, Cursor position is focus position of excitation laser.

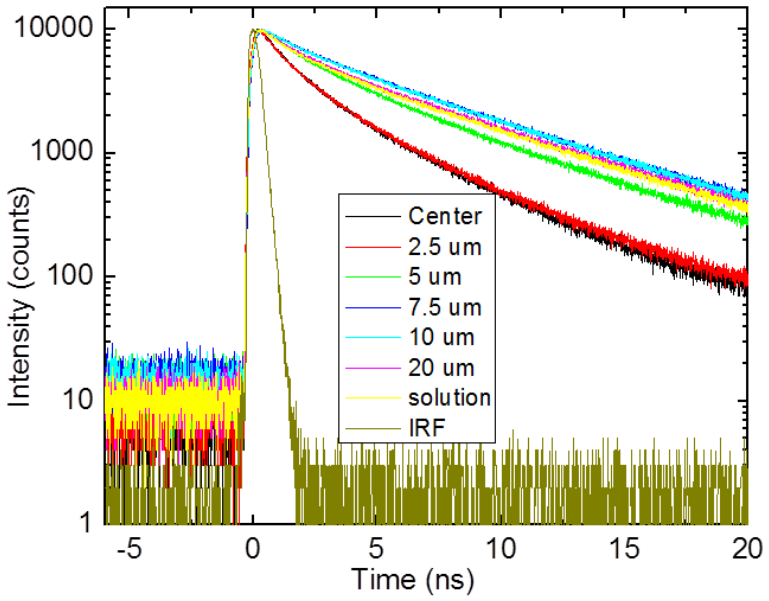

Figure 5.24 Decay curves measured at different position. VDP-PNIPAM was dissolved in H_2O. Phase transition was induced by 200 mW trapping laser. Fluorescence was excited by 375 nm at 12 μW.

Table 5.6. The lifetime value of decay curve at different position far from phase transition center.

	center	2.5 μm	5 μm	7.5 μm	10 μm	20 μm
A_1 (%)	30.6	34.5	49.1	61.5	69.2	61.1
τ_1 (ns)	5.2	5.3	6	6.5	6.8	6.8
A_2 (%)	69.4	65.5	50.9	38.5	30.8	38.9
τ_2 (ns)	1.4	1.5	1.7	1.7	1.7	1.4

Figure 5.23 and 5.24 show the results at different excitation position from the center to far from the center of phase transition particle formed in H_2O solution by focusing 200 mW of trapping laser. Excitation was done by 375 nm femtosecond

pulse laser and laser power is 12 μW. Focus position of excitation laser was fixed and trapping laser was changed. The distance between two lasers is shown in Figure 5.23. The results can be separated to two parts. When measuring in particle, the lifetime decay are the same and shorter than that measured out of phase transition particle. It means in particle, the dehydration degree of polymer chain does not have obvious difference, but rather homogeneous. When we measured the fluorescence decay at out of particle, fluorescence decay was almost similar as what we observed in bulk solution's fluorescence dynamics. Thus we can conclude that outside of the phase transition region even very near of the edge of the particle, which is shown as 5 μm data in the experiment, is same as non-phase transition region in bulk solution.

6. Two color laser-induced phase transition of PNIPAM and VDP-PNIPAM

As we mentioned in the previous chapter, we found very interesting phase transition behavior which is induced by irradiating second weak UV laser. We will discuss this two color induced phase transition in this chapter.

6.1 Blue laser induce phase transition expansion

Figure 6.1 shows typical behavior when we introduce weak UV laser in addition to NIR trapping laser. Initially formed particle by NIR trapping laser became larger by irradiating 325 nm UV laser as shown in Figure 6.1. Particle size became more than three times larger than initial size by UV irradiation. It should be emphasized that the laser fluence of trapping laser and UV laser is obviously different; laser fluence of trapping and UV lasers are in the order of 100 MW/cm^2 and 0.1 W/cm^2, respectively. The second beam is much weaker than that of trapping laser by 8 to 10 orders of magnitude. Particle size was shrunk when we turned off UV laser and returned almost similar size as initial particle size which formed by only NIR trapping laser as shown in Figure 6.1 and 6.2. We also observed particle size can be varied reversibly by turn on/off UV laser. It indicates that observed two color laser induced particle size change is not due to chemical reaction such as cross-linking or additional polymerization, but

probably due to the physical interaction change of polymer chains such as dehydration induced phase separation.

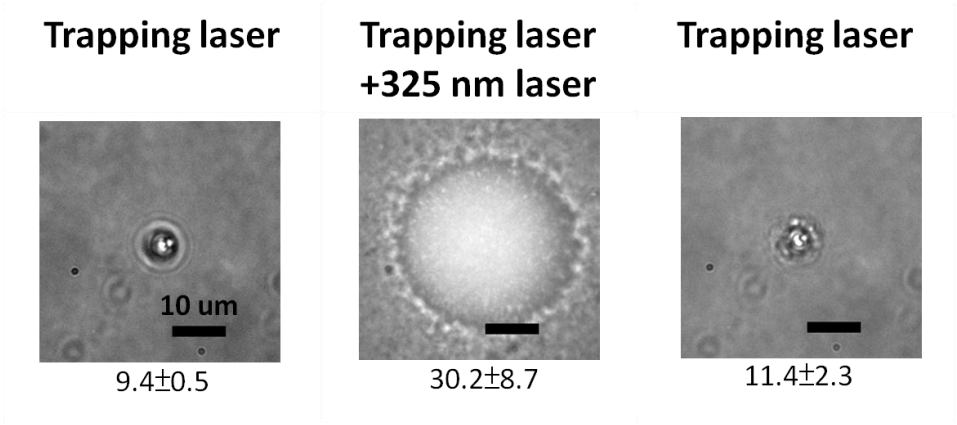

Figure 6.1 Phase transition of VDP- PNIPAM induced by (a) only trapping laser and (b) additional UV laser and (c) again only trapping laser. VDP-PNIPAM in H_2O solution was used. Trapping laser power was 200 mW and UV laser power was 15 mW.

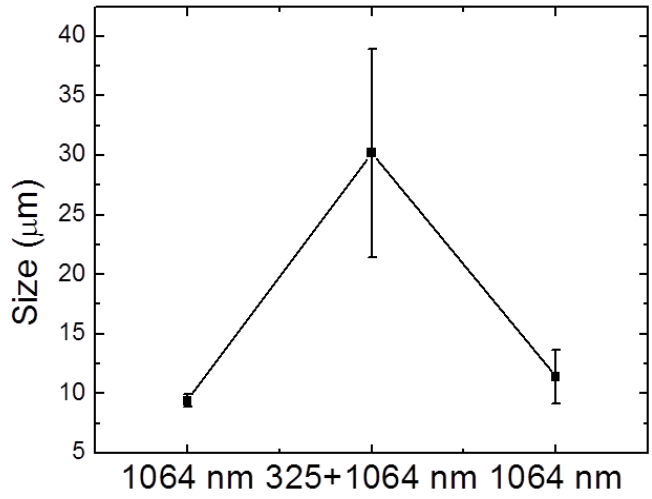

	Trapping laser	Trapping laser +325 nm laser	Trapping laser
Size (μm)	9.4±0.5	30.2±8.7	11.4±2.3

Figure 6.2 Particle size change by turn on/off of 325 nm laser (upper panel) and size at each conditions (lower panel).

We also examined two color induced phase transition of PNIPAM which does not have VDP molecule in polymer chain. We used same laser power as well as in the case depicted in Figure 6.1; t trapping laser and UV laser is 200 mW and 15 mW. By irradiating UV laser, we observed the size change, however the increment of the size is negligibly small compared with VDP-PNIPAM as shown in Figure 6.3 and 6.4. Particle size change in VDP-PNIPAM was 10~20 μm, meanwhile PNIPAM showed just only 1~2 μm change. It is quite negligible compared with that observed in VDP-PNIPAM. It should be noted that we irradiate only UV laser to the solution, no

particle formation and expansion was observed. Interesting point of this phenomenon is that we need to introduce trapping laser and excitation laser simultaneously. If we just use one of them, no particle expansion was observed.

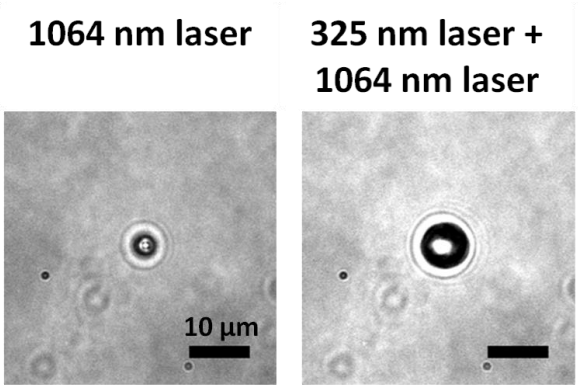

Figure 6.3 Phase transition of PNIPAM induced by trapping laser (a) and UV and trapping laser (b) in H_2O solution. Trapping laser power was 200 mW and UV laser power was 15 mW.

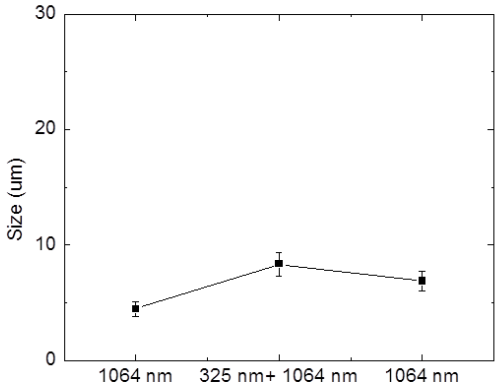

	Trapping laser	Trapping laser +325 nm laser	Trapping laser
size (μm)	**4.5±0.6**	**8.3±1.0**	**6.8**

Figure 6.4 Particle size change of PNIPAM by turn on/off excitation laser in H_2O solution (upper panel). Size at each conditions (lower panel).

6.2 UV laser power dependence of particle expansion in VDP-PNIPAM phase transition

To clarify the reason of observed novel phase transition phenomenon with two color lasers, we examined further experiments. First, we check the excitation laser power dependence of phase transition expansion. There are two purposes for this experiment. First, to know how excitation light power affect to the phase transition particle size change. Second, to know the laser fluence threshold of expansion effect because one of our interest is phase transition induced by "photon pressure".

The results of laser power dependence experiments are shown in Figure 6.5 and 6.6 for H_2O solution and Figure 6.7 and 6.8 for D_2O solution, respectively. Trapping laser power was set to 200 and 600 mW in H2O and D_2O, respectively, with following to the previous experimental results. The phase transition behavior in time and size under examined laser powers in two different solutions are very similar.

In the power dependence experiments, we found that particle size changed depending upon UV laser power. The particle size was enlarged by increasing the UV power and particle size expansion diminished by decreasing. We could see particle size expansion more than 1 mW of UV laser. Thus threshold laser power for expansion was considered as 1 mW.

We also found that the phase transition expansion is more efficiently occur in D_2O than in H_2O solution under same excitation laser power. Here sample concentration was the same and excitation laser power was same. Just only trapping laser power was different. We observed very vigorous phase transition and large particle formation when very high power trapping laser irradiated to PNIPAM in H_2O. At such high laser power we observed similar large particle and surrounding small particles. It implies quite strong heating effect affect to phase transition. However trapping laser power dependent heating effect has not examined yet and further detailed study should be necessary.

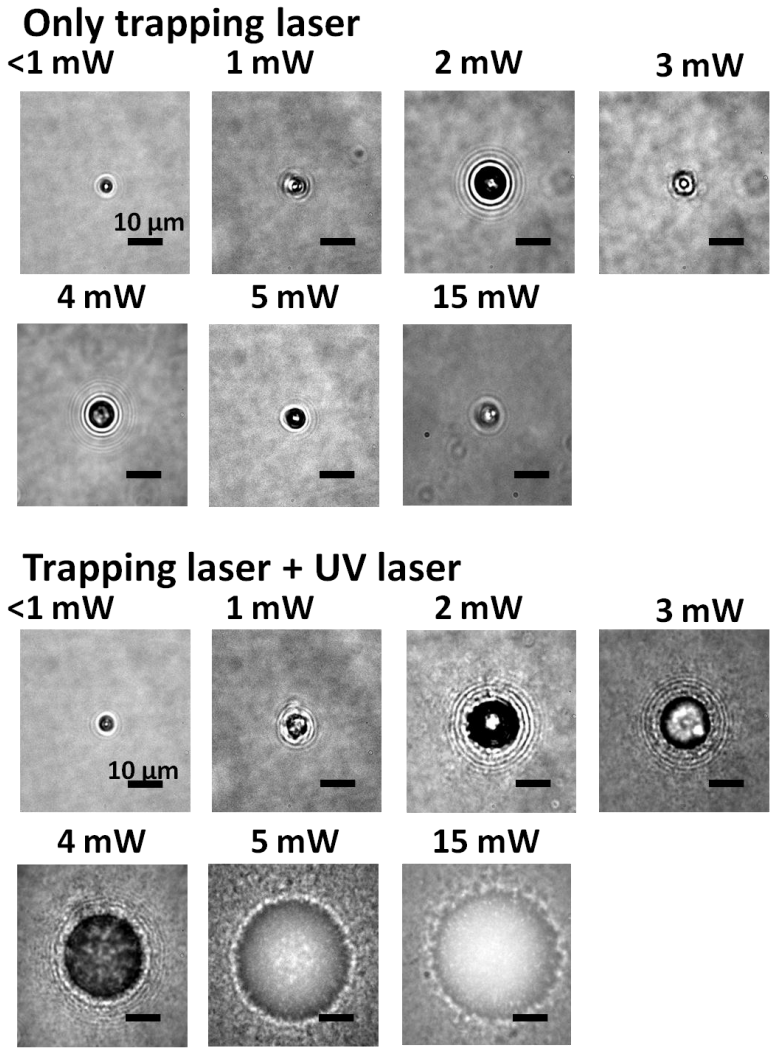

Figure 6.5 Pictures of phase transition particles at each excitation laser power in H_2O solution. (a) ~ (g) are the particles formed by trapping laser and their corresponding two colors laser expansion phase transition images are in (h) ~ (n). Trapping laser power= 200 mW.

Table 6.1 Mean size value of phase transition under each excitation power.

Power	< 1 mW	1 mW	2 mW	3 mW	4 mW	5 mW	15 mW
Only trapping laser(µm)	6.2±0.9	10.2±0.3	10.6±2.6	8.2±0.9	8.6±1.2	8.4±0.9	9.4±0.5
Trapping + UV laser(µm)	6.2±0.9	10.8±0.5	12.1±3.5	17.6±8,5	27.4±5.5	27.0±9.9	30.2±8.7

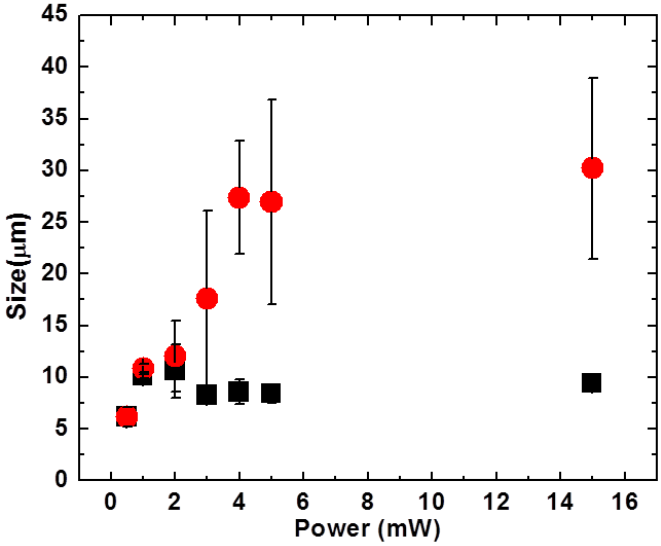

Figure 6.6 Particle size change at each excitation laser power in H_2O solution. Trapping laser power =200 mW. (■) for trapping laser and (●) for two color lasers irradiation.

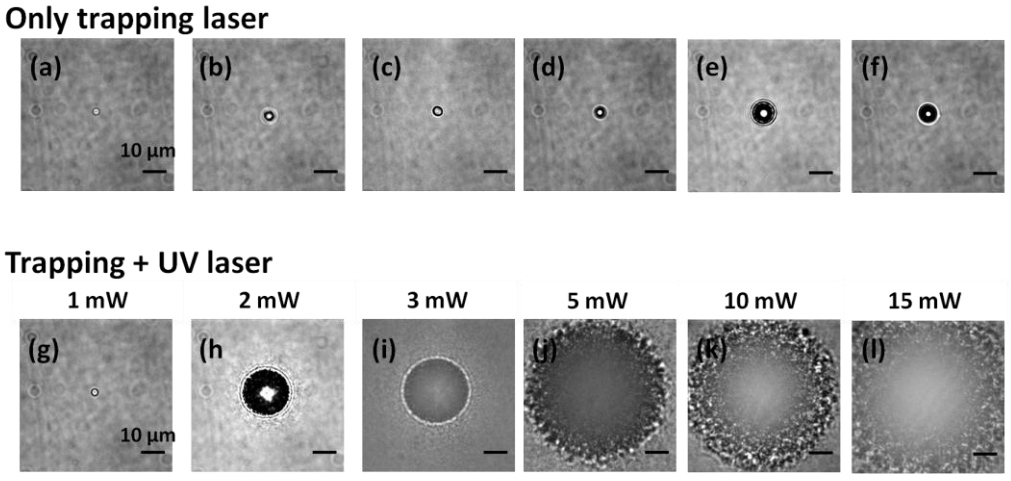

Figure 6.7 Pictures of phase transition particles at each excitation laser power in D_2O solution. (a) ~ (f) are the particles formed by trapping laser and their corresponding two colors laser expansion phase transition images are in (g) ~ (l). Trapping laser power =600 mW.

Table 6.2 Mean size value of phase transition under each excitation power.

Power	1 mW	2 mW	3 mW	4 mW	5 mW	15 mW
Only trapping laser	6.7±1.0	11.5±2.9	6.9±1.4	9.5±3.0	10.4±3.4	9.7±0.5
Trapping + UV laser	7.0±1.0	21.2±2.9	37.3±21.8	50.1±20.0	>65	>65

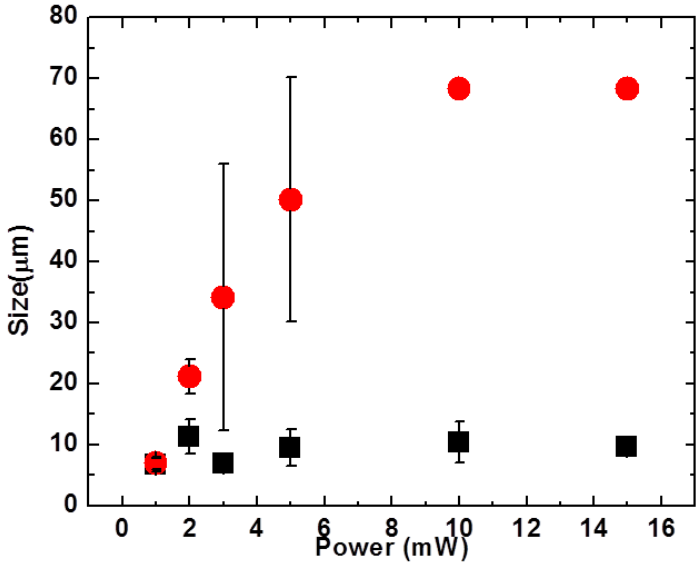

Figure 6.8 Particle size change at each excitation laser power in D_2O solution. Trapping laser power = 600 mW. (■) for trapping laser and (●) for two color lasers irradiation.

6.3 The excitation wavelength dependence for two color effect

For the two color laser induced expansion effect, we need to irradiate sample with two different lasers simultaneously, and then the particle show the expansion. If just one laser, the expansion does not take place. As we show in Figure 6.9, the absorption and fluorescence spectra of VDP-PNIPAM, 325 nm laser light well corresponds to the

absorption band of VDP. It implies that the overlap of second excitation laser light wavelength and absorption wavelength of the molecule has some relationship. Here we will examine wavelength effect for particle expansion by using different wavelength laser light. We employ 375 nm light from mercury lamp obtained by using band-pass filter which bandwidth is 15 nm. A 405 and 488 nm diode laser output were also used as light source. For those experiments, the excitation light power is set as 15 mW for all light source. All of those experiments were done at wide-field illumination condition.

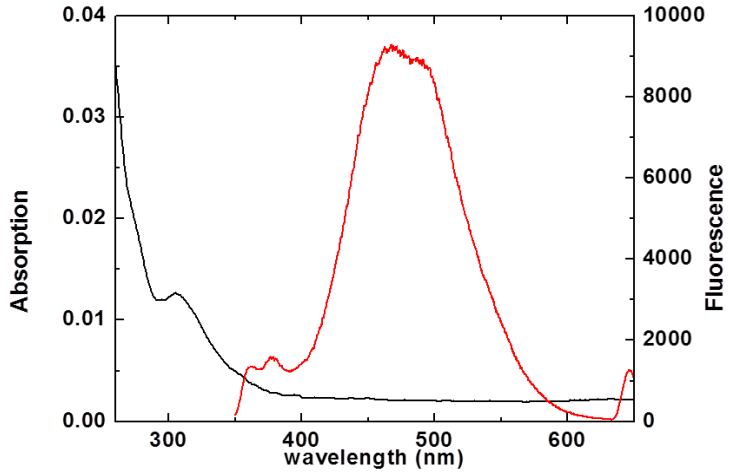

Figure 6.9 Absorption and emission spectrum of VDP-PNIPAM in H_2O solution. Concentration= 0.01 wt %. Excitation wavelength for emission spectrum: 325

As shown in Figure 6.10 and 6.11, we could not see phase transition expansion except 325 nm light. In D_2O solution with 488 nm laser, it seems that the particle enlarged after 488 nm, however the size did not change even after cut 488 nm irradiation. Slight change of the particle size was due to the long time NIR irradiation

not due to second 488 nm light. Particle size change at each laser wavelength are summarized in Figure 6.12 and Table 6.3. Wavelength dependence results strongly suggest that the expansion phenomenon is induced by the light absorbed by the VDP molecule.

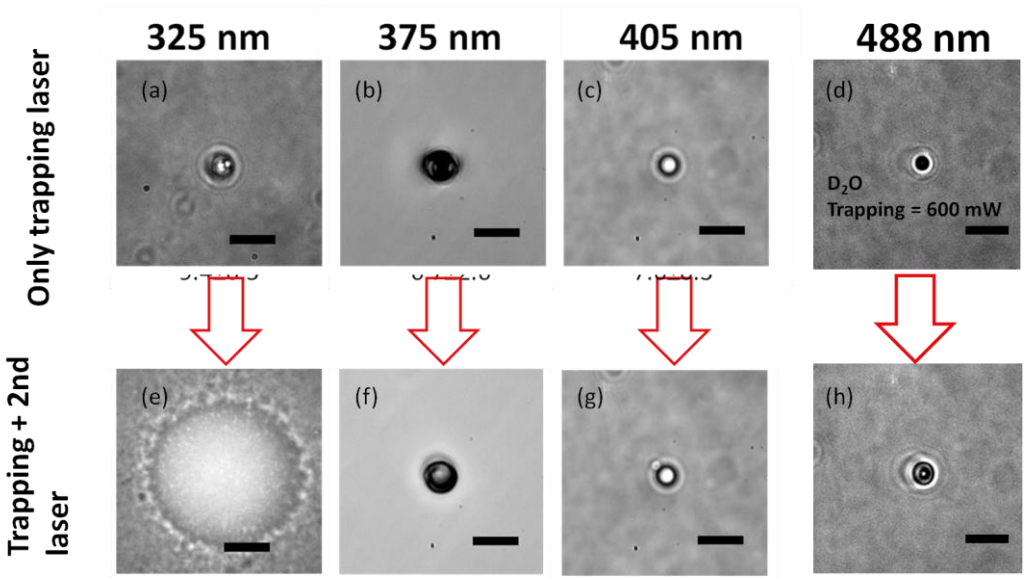

Figure 6.10 Wavelength dependence of phase transition expansion in H_2O solution. (a)~ (d) are phase transition induced by only NIR trapping laser. (e) ~ (f) are phase transition irradiated by second light with 325, 375, 405 and 488 nm, respectively. Graph (d) and (f) are recorded in D_2O solution. Trapping laser power was 200 mW in H_2O and 600 mW in D_2O. All the excitation laser power was 15 mW.

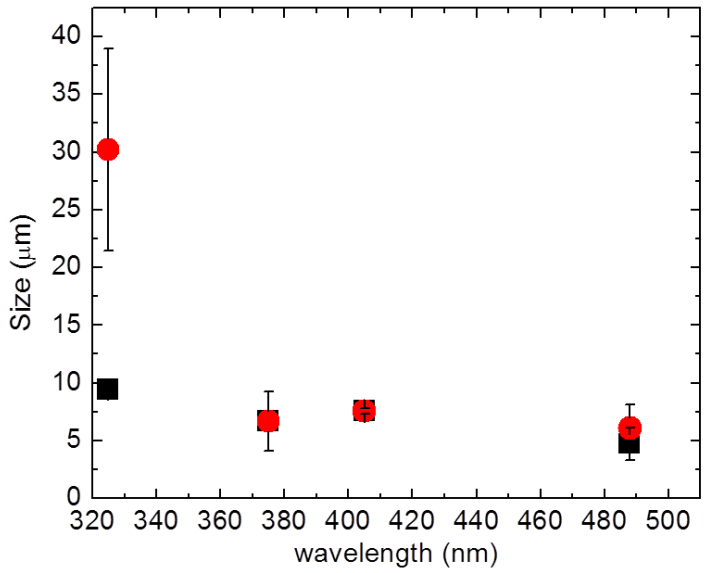

Figure 6.11 Excitation wavelength dependence of VDP-PNIPAM phase transition expansion. The excitation light power at each wavelength is 15 mW. (■) for trapping laser and (●) for two color lasers irradiation.

Table 6.3 Size of particles induced by trapping and two color laser irradiation.

wavelength(nm)	325 nm	375 nm	405 nm	488 nm(D_2O)
Trapping size(μm)	9.4±0.5	6.7±2.6	7.6±0.3	4.7±1.4
Two color laser phase transition (μm)	30.2±8.7	6.72.6	7.6±0.3	6.1±2.1

6.4 Proposed mechanism of two color laser induced phase transition expansion

Comparisons of two color phase transition of non-labeled PNIPAM and VDP-PNIPAM strongly suggest that the phase transition expansion is related to the

existence of VDP. Wavelength dependence indicates importance to use the light which is overlapped with absorption band of chromophore.

The phase transition expansion of VDP-PNIPAM is dramatically larger than PNIPAM phase transition when irradiated with trapping laser and blue laser. Here, we also did the experiment without trapping laser to be reference. It did not show any change by irradiate blue laser even for a long time. That means the phase transition expansion need both two color laser irradiate simultaneously.

Here we can propose two possible reasons for two color laser induced phase transition expansion. One is a resonance effect and another is a photothermal heating effect. An enhanced mechanical interaction between an electromagnetic field and a nanoscopic object near electronic resonance has predicted by theoretical calculations.[51, 52] It suggests that if the wavelength of trapping laser is overlapped with an electronic absorption of the object which will be trapped, stronger mechanical force will be exerted to that object and trapping force will be enhanced. It has been experimentally observed by under optical trapping conditions. Hosokawa et al. has reported resonance laser enhanced biased diffusion of dye-doped polymer nanoparticle which size is 40 nm.[53] They introduced a 1064-nm NIR trapping laser and weak 532 nm laser light for fluorescence excitation to dye-doped nanoparticle dispersed solution and measured diffusion constant of the particles with or without

resonant light by using FCS. It should be noted that 532 nm fluorescence excitation laser is overlapped with the absorption band of doped dye. They observed clear difference in diffusion time when they introduced resonant second laser although the power of resonant light was very low which was in the range of μW. We can notice that an interesting coincidence between their result and ours in terms of the laser condition. They used ~MW/cm^2 trapping laser and much weaker second resonance laser which power density was ~kW/cm^2 to sub ~ kW/cm^2. We observed similar enhancement-like phenomena even we used much lower power density of second UV laser. Another example of resonance enhanced trapping has reported for the trapping study on protein in solution.[54] They examined laser trapping of several protein molecules such as lysozyme, cytochrome c and myoglobin. They observed rapid molecular assembly formation in cytochrome c and myoglobin, but not in lysozyme. They attributed observed enhancement of trapping of cytochrome c and myoglobin to the resonance enhancement of trapping of molecules by two-photon absorption of these proteins. These proteins possess heme in their structure which has electronic absorption band around 500-600 nm region. In the experiment they used ~MW/cm^2 level of power density trapping laser which is sufficiently high fluence that we can expect two-photon absorption of the molecules. Thus they attributed observed enhancement of trapping and formation of assembly due to the resonance effect.

In our experiment we used intense NIR trapping laser and weak UV laser as well as first example as depicted in Figure 6.12. The wavelength of UV laser is overlapped with electronic transition band of labeled fluorophore, VDP, in the polymer molecule. Wavelength effect of second laser by changing its wavelength clearly showed no particle enlargement at 375, 405 and 488 nm at these wavelengths VDP's absorption coefficient is extremely low as we can see in the absorption spectrum. Based on these results we can propose resonance enhancement of trapping of VDP-PNIPAM as one of the reason of observed two color laser enhanced phase transition and particle enlargement.

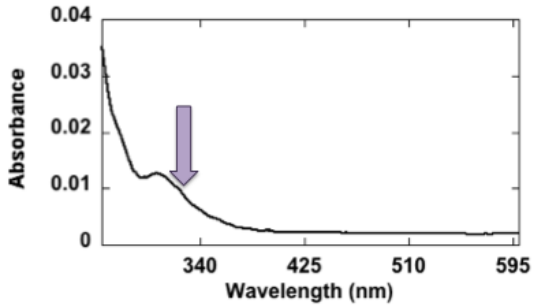

Figure 6.12 Absorption spectrum of VDP-PNIPAM. An arrow in the figure indicates the wavelength of UV laser used in our experiments which has large overlap with electronic transition band of labeled fluorophore.

Another possible reason, photothermal heating, is also related to the absorption of labeled fluorophore VDP. When we introduce 325 nm excitation light, VDP-PNIPAM

will be excited to lowest singlet excited state, i.e. S_1 state, and then excited VDP-PNIPAM transfer to ground state with emitting fluorescence, without emitting by vibronically or through triplet state, and so on, "without" trapping laser. However if NIR trapping light coexist with 325 nm light, NIR light can be absorbed by excited VDP-PNIPAM and it will be excited to higher singlet excited state, S_n state. Typically an excited state lifetime of S_n state is quite short and $S_n \rightarrow S_1$ relaxation occurs at the time scale of picoseconds with vibronically in which process photoexcitatin energy will be converted to thermal energy due to the vibronic relaxation of the molecule; namely it generates a heat. Molecules returned from S_n to S1 state are still exposed to the intense NIR light even after relaxation from higher excited singlet state, and these molecules will be excited and may repeat the same excitation/relaxation process and, most importantly, they generate heats on this cyclic $Sn \rightarrow S_1$ excitation/relaxation process as depicted Figure 6.13. Similar photothermal energy conversion with two laser has reported for anthracene-doped polystyrene films. Fukumura et al. suggested cyclic multiphoton absorption in excited state as well as we mentioned above.[55] Thus once excited states are formed, it works as an efficient photothermal converter with raising local temperature and it can induce further phase transition in a wider region. Again, by changing the excitation laser power, we observed obvious change of the phase transition enhancement. Enhancement of the phase transition efficiency

strongly depends on whether second light has overlap with absorption band of VDP. Additionally, we observed clear difference of the particle size change rate in H_2O and D_2O. VDP-PNIPM/D_2O showed larger change of the particle size under the same UV light power. We used different laser power in H_2O and D_2O since a heat generation ration depends on the solvent and we need much intense NIR laser in D_2O case. As we described above, how much heat will be generated will strongly depend on how efficiently multiphoton absorption will occur in excited state. Therefore we assume that higher power density trapping laser irradiation with resonant UV laser can enhance more heat generation. Of course higher intensity of UV laser also enhance heat generation since we can increase the number of excited VDP molecule by using more excitation photons. It can concisely explain observed two color laser induced enhancement of phase transition.

At the moment we cannot declare which process is correct or not since both possibility can work together in examined conditions. It should be necessary to examine some more experiments for example by changing excitation UV laser wavelength within absorption band, change the chromophore or use non-covalently bonded chromophric system and so on. Further investigation is going on.

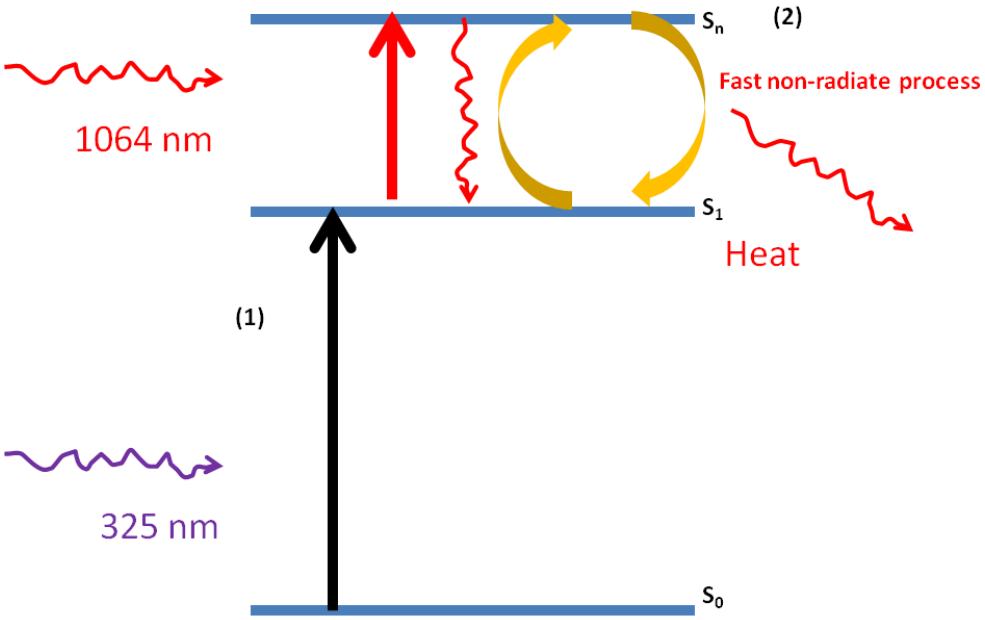

Figure 6.13 Schematic drawing of photothermal effect induced by multiphoton absorption in excited state. Here we omit relaxation path through triplet state in this scheme.

7. Summary

In this study, we have studied the phase transition dynamics of PNIPAM and fluorescently labeled PNIPAM, VDP-PNIPAM, with time- and space-resolved fluorescence microscopy combining with laser trapping technique. Phase transition of PNIPAM molecule will be induced by focusing NIR trapping laser into the PNIPAM solution. Laser irradiation induced micrometer-sized particle formation which can be interpreted due to mainly temperature elevation in H_2O and both temperature and photon pressure of focused trapping laser in D_2O.

We combined the wide-field imaging, confocal spectrum measurement and fluorescence lifetime measurement with TCSPC at the trapping laser spot to elucidate phase transition dynamics. Time- and space-resolved fluorescence microspectroscopy with VDP-PNIPM gave us quantitative information of phase transition dynamics which we cannot obtain just only using conventional imaging methods.

We also found novel phase transition behavior. By combining the trapping laser with additional UV excitation laser, we observed unconventional enhancement of phase transition. This phenomenon can be induced only by simultaneous introduction of two lasers. We experimentally studied this phenomenon in detail and proposed the mechanism of it.

In chapter three, we discuss the thermal effect of solvent and substrate. For

trapping experiment, we also need to take care about the absorption of solvent and substrate because heat is one issue in our study. We check the thermal effect which comes from the absorption of solvent by changing solvent to D_2O. In D_2O solution, the phase transition will not appear by using low power laser which can induce phase transition in H_2O. That means the phase transition in H_2O is mainly due to heating effect. For the heating effect from the absorption of substrate, it can be neglected by changing the substrate to quartz. The difference caused by heating effect from substrate is like change the system temperature.

In chapter four we introduced our FLIM system. It enables us to measure fluorescence dynamics by measuring fluorescence lifetime with TCSPC. By using FLIM we can observe phase transition dynamics by probing the excited state fluorescence dynamics of probe chromophore, VDP. Spatial resolution of our system is determined to 280 nm for lateral plane. We can measure fluorescence spectra and images simultaneously in addition to fluorescence decay curves. It will give us more clear insight for phase transition dynamics of PNIPAM.

In chapter five, we studied phase transition dynamics by using VDP-PNIPAM as molecular probe and by probing fluorescence image, spectrum, and lifetime. Simultaneous observation of image, spectrum and decay curve is quite powerful method. We can visualize the phase transition dynamics with higher sensitivity and

time resolution. We observed that molecular environment did not returned to the original coil state even after disappearing of phase transition particle. It could not observed just only conventional bright field imaging but the combination multimodal detection enabled it.

In chapter six, we discussed two color laser induced unusual phase transition behavior. The expansion of VDP-PNIPAM phase transition particle is explained with the interaction between electronic transition band of laveled fluorophore and irradiated two lights, UV excitation laser and NIR trapping laser. We proposed two possible pathway for the particle expansion by resonance effect and photothemal effect. Both mechanisms are acceptable to explain observed particle expansion and we could not conclude which mechanism induced observed enhanced phase transition behavior. However Experimental results gave us many clues to solve this puzzle and we are doing further experiments to clarify the mechanism of this interesting phenomenon.

Reference

[1] H.G. Schild, "Poly (N-Isopropylacrylamide) - experiment, theory and application", Prog. Polym. Sci., **17**, 163-249, 1992.

[2] E.S. Gil, S.M. Hudson, "Stimuli-reponsive polymers and their bioconjugates", Prog. Polym. Sci., **29**, 1173-1222, 2004.

[3] A. Hoffman, P. Stayton, "Bioconjugates of smart polymers and proteins: synthesis and applications", Macromol Symp, **207**, 139-152, 2004.

[4] E.I. Tiktopulo, V.E. Bychkova, J. Ricka, O.B. Ptitsyn, "Cooperativity of the coil-globule transition in a homopolymer - microcalorimetric study of poly(N-isopropylacrylamide)", Macromolecules, **27**, 2879-2882, 1994.

[5] E.I. Tiktopulo, V.N. Uversky, V.B. Lushchik, S.I. Klenin, V.E. Bychkova, O.B. Ptitsyn, "Domain coil-globule transition in homopolymers", Macromolecules, **28**, 7519-7524, 1995.

[6] J. Ricka, M. Meewes, R. Nyffenegger, T. Binkert, "ntermolecular and intramolecular solubilization - collapse and expansion of a polymer-chain in surfactant solutions", Phys. Rev. Lett., **65**, 657-660, 1990.

[7] K. Kubota, S. Fujishige, I. Ando, "Single-chain transition of poly(N-isopropylacrylamide) in water", J. Phys. Chem., **94**, 5154-5158, 1990.

[8] T. Tokuhiro, T. Amiya, A. Mamada, T. Tanaka, "NMR study of poly(N-isopropylacrylamide) gels near phase transition", Macromolecules, **24**, 2936-2943, 1991.

[9] H. Ohta, I. Ando, S. Fujishige, K. Kubota, "Molecular-motion and H-1-NMR relaxation of aqueous poly(N-isopropylacrylamide) solution under high pressure", J. Polym. Sci. Pt. B-Polym. Phys., **29**, 963-968, 1991.

[10] M. Schonhoff, A. Larsson, P.B. Welzel, D. Kuckling, "Thermoreversible polymers adsorbed to colloidal silica: A H-1 NMR and DSC study of the phase transition in confined geometry", J. Phys. Chem. B, **106**, 7800-7808, 2002.

[11] F.M. Winnik, "Fluorescence studies of aqueous-solutions of poly(N-isopropylacrylamide) below and above their LCST", Macromolecules, **23**, 233-242, 1990.

[12] T. Binkert, J. Oberreich, M. Meewes, R. Nyffenegger, J. Ricka, "Coil globule transition of poly(N-isopropylacrylamide) - a study of segment mobility by fluorescence depolarization", Macromolecules, **24**, 5806-5810, 1991.

[13] S. Fujishige, K. Kubota, I. Ando, "Phase-transition of aqueous-solutions of poly(N-isopropylacrylamide) and poly(N-isopropylmethacrylamide)", J Phys Chem, **93**, 3311-3313, 1989.

[14] C. Boutris, E.G. Chatzi, C. Kiparissides, "Characterization of the LCST

behaviour of aqueous poly(N-isopropylacrylamide) solutions by thermal and cloud point techniques", Polymer, **38**, 2567-2570, 1997.
[15] F.M. Winnik, "Phase-transition of aqueous poly-(N-isopropylacrylamide) solutions - a study by nonradiative energy-transfer", Polymer, **31**, 2125-2134, 1990.
[16] K. Chan, R. Pelton, J. Zhang, "On the formation of colloidally dispersed phase-separated poly(N-isopropylacrylamide)", Langmuir, **15**, 4018-4020, 1999.
[17] V. Aseyev, S. Hietala, A. Laukkanen, M. Nuopponen, O. Confortini, F.E. Du Prez, H. Tenhu, "Mesoglobules of thermoresponsive polymers in dilute aqueous solutions above the LCST", Polymer, **46**, 7118-7131, 2005.
[18] A.V. Gorelov, A. DuChesne, K.A. Dawson, "Phase separation in dilute solutions of poly (N-isopropylacrylamide)", Physica A, **240**, 443-452, 1997.
[19] C. Wu, W. Li, X.X. Zhu, "Viscoelastic effect on the formation of mesoglobular phase in dilute solutions", Macromolecules, **37**, 4989-4992, 2004.
[20] K. Van Durme, G. Van Assche, B. Van Mele, "Kinetics of demixing and remixing in poly(N-isopropylacrylamide)/water studied by modulated temperature DSC", Macromolecules, **37**, 9596-9605, 2004.
[21] K. Van Durme, L. Delellio, E. Kudryashov, V. Buckin, B. Van Mele, "Exploration of high-resolution ultrasonic spectroscopy as an analytical tool to study demixing and remixing in poly(N-isopropyl acrylamide)/water solutions", J. Polym. Sci., Part B: Polym. Phys., **43**, 1283-1295, 2005.
[22] P.V. Yushmanov, I. Furo, I. Iliopoulos, "Kinetics of demixing and remixing transitions in aqueous solutions of poly(N-isopropylacrylamide): A temperature-jump H-1 NMR study", Macromol Chem Physic, **207**, 1972-1979, 2006.
[23] Y. Tsuboi, Y. Yoshida, K. Okada, N. Kitamura, "Phase separation dynamics of aqueous solutions of thermoresponsive polymers studied by a laser T-jump technique", J. Phys. Chem. B, **112**, 2562-2565, 2008.
[24] K. Iwai, K. Hanasaki, M. Yamamoto, "Fluorescence label studies of thermo-responsive poly(N-isopropylacrylamide) hydrogels", J. Lumin., **87-89**, 1289-1291, 2000.
[25] K. Iwai, N. Matsumoto, M. Niki, M. Yamamoto, M. Hiroshi, N. Hachiro, K. Masahiro, "Fluorescence probe studies of thermosensitive N-isopropylacrylamide copolymers in aqueous solutions", Mol. Cryst. Liq. Cryst. Sci. Technol., Sect. A, **314-15**, 355-360, 1998.
[26] Y. Matsumura, K. Iwai, "Synthesis and thermo-responsive behavior of fluorescent labeled microgel particles based on poly(N-isopropylacrylamide) and its related polymers", Polymer, **46**, 10027-10034, 2005.
[27] G. Graziano, "On the temperature-induced coil to globule transition of poly-N-isopropylacrylamide in dilute aqueous solutions", Int. J. Biol. Macromol., **27**,

89-97, 2000.
[28] H.G. Schild, M. Muthukumar, D.A. Tirrell, "Cononsolvency in mixed aqueous-solutions of poly(N-isopropylacrylamide)", Macromolecules, **24**, 948-952, 1991.
[29] E.C. Aguilar M. R., Gallardo A., Vázquez B., and Román J. S., "Smart polymers and their applications as bomaterials", Toc. Tissue Eng., **3**, 27., 2007.
[30] J. Kost, R. Langer, "Responsive polymeric delivery systems", ADV DRUG DELIVER REV, **46**, 125-148, 2001.
[31] S.L. Gras, T. Mahmud, G. Rosengarten, A. Mitchell, K. Kalantar-Zadeh, "Intelligent control of surface hydrophobicity", Chemphyschem, **8**, 2036-2050, 2007.
[32] M. Ishikawa, H. Misawa, N. Kitamura, H. Masuhara, "Poly(N-isopropylacrylamide) microparticle formation in water by infrade laser-induced photothermal phase-transition", Chem. Lett., 481-484, 1993.
[33] J. Hofkens, J. Hotta, K. Sasaki, H. Masuhara, K. Iwai, "Molecular Assembling by the Radiation Pressure of a Focused Laser Beam: Poly(N -isopropylacrylamide) in Aqueous Solution", Langmuir, **13**, 414-419, 1997.
[34] J. Hofkens, J. Hotta, K. Sasaki, H. Masuhara, K. Iwai, "Molecular assembling by the radiation pressure of a focused laser beam: Poly(N-isopropylacrylamide) in aqueous solution", Langmuir, **13**, 414-419, 1997.
[35] A. Ashkin, "Acceleration and trapping of particles by radiation pressure", Phys. Rev. Lett., **24**, 24-27, 1970.
[36] A. Ashkin, J.M. Dziedzic, J.E. Bjorkholm, S. Chu, "Observation of a single-beam gradient force optical trap for dielectric particles", Opt Lett, **11**, 288, 1986.
[37] H. Kojima, E. Muto, H. Higuchi, T. Yanagida, "Mechanics of single kinesin molecules measured by optical trapping nanometry", Biophys. J., **73**, 2012-2022, 1997.
[38] F.C.d. H. Masuhara, N. Kitamura, and N. Tamai, , "Microchemistry: Spectroscopy and Chemistry in Small Domains", 1994.
[39] Y. Tsuboi, T. Shoji, N. Kitamura, "Crystallization of lysozyme based on molecular assembling by photon pressure", Jpn J Appl Phys 2, **46**, L1234-L1236, 2007.
[40] K.C. Neuman, S.M. Block, "Optical trapping.", Rev. Sci. Instrum., **75**, 2787-2809, 2004.
[41] A. Ashkin, "Forces of a single-beam gradient laser trap on a dielectric sphere in the ray optics regime", Biophys J, **61**, 569-582, 1992.
[42] A. Ashkin, L. Fellow, "Small-neutral particle , atoms , and molecules", Quantum, **6**, 841-856, 2000.
[43] K. Iwai, N. Matsumoto, M. Niki, M. Yamamoto, "Fluorescence probe studies of

thermosensitive N−isopropylacrylamide copolymers in aqueous solutions", Mol. Cryst. Liq. Cryst. Sci. Technol., Sect. A, **315**, 53-58, 1998.
[44] S. Ito, T. Sugiyama, N. Toitani, G. Katayama, H. Miyasaka, "Application of fluorescence correlation spectroscopy to the measurement of local temperature in solutions under optical trapping condition", J. Phys. Chem. B, 2365-2371, 2007.
[45] J.R. Lakowicz, "Time-Domain Lifetime Measurements", Principles of Fluorescence Spectroscopy Third Edition, 59, 2006.
[46] J.R. Lakowicz, "Fluorescence-Lifetime Imaging Microscopy", Principles of Fluorescence Spectroscopy Third Edition, 15, 2006.
[47] R.K. Kannadorai, U.S. Dinish, C.Y. Fu, M. Olivo, A. Asundi, "Fabrication and characterization of mono-layered polystyrene beads using nanosphere lithography (NSL) for metal-enhanced fluorescence (MEF)", Proc. of SPIE, **7522**, 752269-752269-752266, 2009.
[48] A. Onkelinx, F.C. DeSchryver, L. Viaene, M. VanderAuweraer, K. Iwai, M. Yamamoto, M. Ichikawa, H. Masuhara, M. Maus, W. Rettig, "Radiative depopulation of the excited intramolecular charge-transfer state of 9-(4-(N,N-dimethylamino)phenyl)phenanthrene", J. Am. Chem. Soc., **118**, 2892-2902, 1996.
[49] A. Onkelinx, G. Schweitzer, F.C. DeSchryver, H. Miyasaka, M. VanderAnweraer, T. Asahi, H. Masuhara, H. Fukumura, A. Yashima, K. Iwai, "Femto- to microsecond excited state relaxation of 9-(4-(N,N-dimethylamino)phenyl)phenanthrene and 4-(9-phenanthryl)-3,5-N,N-tetramethylaniline", J. Phys. Chem. A, **101**, 5054-5062, 1997.
[50] H. Inoue, K. Katayama, K. Iwai, A. Miura, H. Masuhara, "Conformational relaxation dynamics of a poly(N-isopropylacrylamide) aqueous solution measured using the laser temperature jump transient grating method", Phys Chem Chem Phys, **14**, 5620-5627, 2012.
[51] T. Iida, H. Ishihara, "Study of the mechanical interaction between an electromagnetic field and a nanoscopic thin film near electronic resonance", Opt. Lett., **27**, 754-756, 2002.
[52] H. Ajiki, T. Iida, T. Ishikawa, S. Uryu, H. Ishihara, "Theory of radiation force on carbon nanotubes", Jpn. J. Appl. Phys., **49**, 2010.
[53] C. Hosokawa, H. Yoshikawa, H. Masuhara, "Enhancement of biased diffusion of dye-doped nanoparticles by simultaneous irradiation with resonance and nonresonance laser beams", Jpn J Appl Phys 2, **45**, L453-L456, 2006.
[54] Y. Tsuboi, T. Shoji, M. Nishino, S. Masuda, K. Ishimori, N. Kitamura, "Optical manipulation of proteins in aqueous solution", Appl. Surf. Sci., **255**, 9906-9908, 2009.
[55] H. Fukumura, H. Masuhara, "The mechanism of dopant-induced laser-ablation -

possibility of cyclim multiphotonic absorption in excited-states", Chem. Phys. Lett., **221**, 373-378, 1994.

Acknowledgement

First and foremost, I want to thank Prof. Masuhara, Prof. Miura. They help me very much for this project. Without them, I can not finish this research. They give me a lot of idea of research and teach me much experiment technique and research attitude. Also, without them, I can not do those experiments with this kind of good experiment condition. I am very happy to have this work in this laboratory. I really learn much in these two years. Besides, I want to thank Prof. Miura, especially. Without him, I can not finish this thesis as good as this. He really help me a lot on every part of my research.

Second, I want to thank thesis reviewers, Prof. Yau Kuan Lee, Prof. Yen-Ju Cheng and also Prof. Masuhara. They give me a lot of good common on my master defence to make this thesis become better. Also, they give me some advise and idea for my research.

Third, I want to thank all the lab members. I am very happy to work with them during these two years. I have very good remember in these two years. They also help me a lot when I doing experiment. If I have some problem, always they can give me good advises.

Finally, I want thank all the members who help me in these two years. Without them, I can not graduate smoothly. Thank you for your help.